DOI: 10.26599/FSHW.2026.9251045

Contents lists available at SciOpen

Food Science and Human Wellness

journal homepage: https://www.sciopen.com/journal/2097-0765

China Food Publishing Co.

Chicory Sesquiterpene Lactones Trained Faeces-derived Extracellular Vesicles Alleviated Ulcerative Colitis by Modulating Gut Microbiota and Bile Acids Metabolism

Tunyu Jian[a,1], Zhen Tang[a, 1], Yuwen Tian[a], Weichen Zhang[a], Xiaoqin Ding[a], Xiuhua Meng[a], Han Lv[a], Bei Tong[a], Yanan Gai[a], Weilin Li[b], Lan Wu[c], Guanting Niu[a*], Jian Chen[a*]

[a] *Jiangsu Key Laboratory for Conservation and Utilization of Plant Resources, Institute of Botany, Jiangsu Province and Chinese Academy of Sciences, Nanjing 210014, China*

[b] *Co-Innovation Center for Sustainable Forestry in Southern China, College of Forestry, Nanjing Forestry University, Nanjing 210037, China*

[c] *Department of Gynecology and Obstetrics, Women's Hospital of Nanjing Medical University, Nanjing Women and Children's Healthcare Hospital, Nanjing 210004, China*

ABSTRACT: The gut microbiota communicates with the host via extracellular vesicles (EVs), offering a promising therapeutic target for ulcerative colitis (UC). This study investigates the therapeutic potential of sesquiterpene lactones (SL) from chicory and the EVs derived from the faeces of SL-treated mice (SL-trained FEVs) in a dextran sulfate sodium (DSS)-induced UC model. Oral administration of SL significantly ameliorated colitis symptoms, reduced intestinal inflammation, preserved intestinal barrier integrity by maintaining tight junction proteins, and attenuated colonic tissue damage. These protective effects were mechanistically linked to the attenuation of gut microbiota dysbiosis and the restoration of bile acid metabolism homeostasis. Notably, gavage of SL-trained FEVs recapitulated the therapeutic benefits of direct SL treatment, demonstrating the critical role of microbiota-derived EVs in mediating SL's effects. Profiling revealed that SL treatment enriched specific microRNAs (e.g., miR-26a-5p, miR-200b-3p, and miR-194-5p) within these FEVs. Both SL and SL-trained FEVs induced comparable and significant shifts in the gut microbiota composition, notably modulating the relative abundance of genera including *Odoribacter*, *Oscillibacter*, *Escherichia-Shigella*, *g-Clostridia_UCG-014_unclassified*, and phyla such as p-Actinobacteriota and p-Patescibacteria. Concomitantly, both interventions significantly altered key bile acid profiles, affecting levels of taurocholic acid (TCA), lithocholic acid (LCA), nor-deoxycholic acid (NorDCA), and taurochenodeoxycholic acid (TCDCA). In conclusion, our findings highlight SL and SL-trained FEVs as promising agents for UC treatment, acting through the coordinated modulation of the gut microbiota-bile acid axis, and propose FEVs as a novel, targeted delivery system for microbiota-based therapeutics.

Keywords Faeces-derived extracellular vesicles, ulcerative colitis, gut microbiota, chicory, miRNA, bile acids

1. Introduction

Ulcerative colitis (UC) is a chronic inflammatory condition of the colon with a rising global incidence, posing a significant challenge to public health due to the lack of universally effective and safe therapeutic

[1] These authors contributed equally to this work.
***Corresponding author**
Dr. Guanting Niu, celianewmit@sina.com
Prof. Jian Chen, chenjian80@aliyun.com

Received 24 January 2025
Received in revised from 6 March 2025
Accepted 3 April 2025

strategies [1]. Current first-line treatments, including corticosteroids and biologic agents such as anti-TNFα antibodies, are often limited by substantial side effects, high costs, and variable patient responsiveness [2]. These limitations underscore the urgent need to develop novel, well-tolerated, and efficacious interventions for UC management.

Accumulating evidence highlights the gut microbiota as a key player in maintaining intestinal homeostasis and modulating host immune function [3-5]. Dysbiosis of the gut microbial community-characterized by altered microbial composition, impaired barrier integrity, and disrupted metabolite production-has been closely linked to the pathogenesis and progression of UC [6-8]. Among the various microbial-derived mediators, extracellular vesicles (EVs) have emerged as critical facilitators of cross-kingdom communication. These nanoscale particles (20–400 nm), secreted by both host and microbial cells, carry diverse bioactive molecules including nucleic acids, proteins, and lipids, and are increasingly recognized for their role in regulating intestinal health [9-11]. Notably, faeces-derived EVs (FEVs) have been shown to influence systemic inflammation, metabolic disorders, and gut barrier function, suggesting their potential as both diagnostic and therapeutic targets in UC [12-14].

Dietary intervention represents a promising approach for modulating gut microbiota and mitigating intestinal inflammation [15-17]. Chicory (*Cichorium intybus* L.), a widely consumed edible plant rich in bioactive compounds such as SL), has demonstrated anti-inflammatory, antioxidant, and gut-modulating properties[18-20]. Our previous studies have confirmed that chicory-derived phenolic acids can ameliorate colitis by reshaping the gut microbiota[21]. Among its constituents, SL particularly those containing an α-methylene-γ-lactone moiety-exhibit potent anti-inflammatory activity through modulation of the NF-κB and NRF2 signaling pathways [22]. However, whether SL from chicory can alleviate UC via regulation of gut microbiota and their derived EVs remains unexplored.

In this study, we hypothesized that chicory-derived SL interact with the gut microbiota to modulate the composition and miRNA cargo of FEVs, thereby exerting protective effects against UC. Using a DSS-induced murine model, we evaluated the therapeutic efficacy of both SL administration and SL-trained FEV transplantation. Our integrated approach combined 16S rRNA sequencing, bile acid metabolomics, and miRNA profiling to elucidate the underlying mechanisms. This work not only provides novel insights into the role of diet-trained FEVs in gut–host communication but also proposes a potential strategy for UC treatment using plant-derived vesicles.

2. Materials and methods

2.1 Materials and reagents

Fresh chicory leaves were harvested from the Nanjing Botanical Garden Mem. Sun Yat-Sen located in Nanjing, Jiangsu, China, and identified by Prof. Bingru Ren, and preserved in the herbarium of the Institute of Botany, Jiangsu Province and the Chinese Academy of Sciences, Nanjing, China, under specimen number 20200402. Dextran sodium sulfate (DSS, molecular weight 36000-50000, 02160110-CF) was obtained from MP Biomedicals (CA, USA). Different concentrations of sucrose (8, 30, 45, and 60 %; R27584, R21504,

R27585, and R27586) were purchased from Shanghai Yuanye Bio-Technology Co., Ltd (Shanghai, China). Tumour necrosis factor-α (TNF-α, E-EL-M3063), interleukin-1β (IL-1β, E-EL-M0037), interleukin-6 (IL-6, E-EL-M0044), and interleukin-18 (IL-18, E-EL-M0730) levels in the serum of mice were detected using ELISA kits purchased from Elabscience Biotechnology Co., Ltd (Wuhan, China). Antibodies ZO-1 (21773-1-AP), E-cadherin (20874-1-AP), Claudin1 (28674-1-AP), Occludin (27260-1-AP), TLR4 (19811-1-AP), NLRP3 (30109-1-AP), NFκB (33259-1-AP), and p-NFκB (82335-1-RR) were purchased from Proteintech Group, Inc. (Wuhan, China). 3,3′-dioctadecyloxacarbocyanine perchlorate (DiO, BL925A), 4',6-diamidino-2-phenylindole (DAPI, BL120A) were obtained from Biosharp (Hefei, China), RNase A (EN0531) was obtained from Thermo Fisher Scientific (Massachusetts, US), and Taurochenodeoxycholic Acid (TCDCA) (HY-N2027) was obtained from MedChemExpress (Shanghai, China).

2.2 Prepared and identified SL from chicory leaves

The preparation of SL was set as follows: The dried leaves of chicory were soaked in 85% ethanol for seven days. Afterward, the extract was filtered and concentrated. Then, D101 macroporous resin was employed to remove most of the saccharides. The resulting 95% ethanol eluent was then concentrated and rehydrated with water before being processed through polyamide resin (30-60 mesh) to adsorb the polyphenols. The fraction eluted with water enriched in Sesquiterpene lactones was referred to as the SL extract. Then, high-performance liquid chromatography (HPLC) and mass spectrometry methods were employed to detect and assess the SL sample.

The assay was conducted using a Dionex Ultimate 3000 HPLC system equipped with a YMC-Pack ODS-AQ column (250 × 4.6 mm, 5 μm, Japan). The mobile phase consisted of acetonitrile (A) and 0.1% formic acid in water (B), with a 1 mL/min flow rate, and was reduced to 0.25 mL/min via a post-column flow splitter prior to MS introduction. The elution program was as follows: 0-40 min, 10-40% A; 40-45 min, 40-50% A; 45-50 min, 50-60% A; 50-52 min, 60-90% A; 52-57 min, 90% A; 57-60 min, 90-10% A; 60-65 min, 10% A. The column temperature was maintained at 25°C, and the injection volume was 10 μL.

2.3 Animals

Male C57BL/6J mice, weighing between 22 and 25 g, were sourced from Changzhou Cavens Lab Animal Co. (Changzhou, China, production license: SCXK(Su) 2021-0013). The mice were housed under controlled conditions: the environmental parameters were set at a temperature of 22 ± 2°C, a relative humidity of 55 ± 5%, and a 12-hour light/dark cycle. And mice had free access to food and water. All the experimental protocols received approval from the Animal Ethics Committee of China Pharmaceutical University (No. 2023-03-004).

2.4 The preventive effect of SL on ulcerative colitis

After a 1-week adaptation period, forty mice were randomly divided into two groups: The normal control group (Control), mice were given normal drinking water (n=10), and the DSS model group (DSS), mice were given 2.5% DSS drinking water (n=30). After 2 days, mice in the DSS group were further divided into 3

subgroups (n=10): (1) DSS model group (DSS), mice were gavaged with PBS; (2) SL low dosage (SLL-DSS), mice were gavaged with 100 mg/kg SL; (3) SL high dosage (SLH-DSS), mice were gavaged with 200 mg/kg SL. Drug administration continued for an additional 5 days. The specific workflow was illustrated in Fig. 2A. All of the doses for mice were selected based on comprehensive pre-experiments. Oral gavage of high-concentration SL (2000 mg/kg) in mice showed no safety concerns, complying with acute toxicity assessment.

2.5 Isolation and purification of FEVs

The donor mice were given 2.5% DSS drinking water and SL (high dosage at 200 mg/kg) for 7 days. Fresh faeces in the colon were collected at the end of the period. To prepare the SL-trained FEVs for transplantation, 1 g Fresh faeces in the colon were suspended in 50 mL phosphate-buffered saline (PBS), homogenized, and centrifuged at 5000 × g for 10 min at 4 °C. Then, the crude FEVs in the supernatant were isolated by ultracentrifugation (Thermofisher Sorvall WX100+, Thermo Scientific, USA, rotor SureSpin 632), with a sucrose density gradient (8, 30%, 45%, and 60%) at 100,000 × g for 2 h. The fraction at the sucrose interfaces between 30-45 % was collected as purified FEVs. Five volumes of PBS were added and ultra-centrifugated (100,000 × g, 2 h) to remove sucrose. The final FEVs pellets were collected, and resuspended in PBS. The protein concentration of FEVs was measured using a BCA kit. The samples were stored at -80°C until further use.

2.6 Morphology characterization and miRNA profiling of FEVs

The morphology of FEVs was obtained using transmission electron microscopy (TEM) with the HT-7700 model from Hitachi, Japan. The size distribution and particle concentration of FEVs were determined using a flow NanoAnalyzer (N30E, NanoFCM, China). This study employed the Exosomal RNA Isolation Kit (NGB-58000, CA) for the preparation of total RNA of FEVs. Sequencing was performed on the Illumina HiSeq 2500 platform using a single-end (SE) configuration with 50 cycles. After sequencing, quality filtering, adapter trimming, and length selection were applied to the single-end sequencing reads using ACGT101-miR (LC Sciences, Houston, Texas, USA). Functional annotation of the differentially expressed miRNAs was performed using Gene Ontology (GO) terms (http://geneontology.org/) and the KEGG pathway (https://www.genome.jp/kegg/).

2.7 Labeling and intestinal uptake of SL-trained FEVs

Purified SL-trained FEVs were incubated with 1 mM DiO at 37°C for 30 min, followed by ultracentrifugation at 100,000 × g for 2 h to remove the unbound dye, yielding DiO-labeled FEVs. Through oral gavage, 50 μg of DiO-labeled SL-trained FEVs were administered to C57BL/6J mice. At the time points of 0, 3, 6, 12, and 24 h, the mice were euthanized, and the small intestines and colons were harvested for imaging analysis to determine the distribution of the DiO-labeled SL-trained FEVs (IVIS Lumina III in vivo imaging system, PerkinElmer, USA).

2.8 Transplantation of SL-trained FEVs in ulcerative colitis mice

Thirty mice from the same source in the same experimenting environment were randomly divided into 2 groups: Normal control group (NC), mice were given normal drinking water (n=10), and DSS model group (DSS), mice were given 2.5% DSS drinking water (n=20). After 2 days, mice in the DSS group were further divided into 2 subgroups (n=10): (1) DSS model group (DSS), mice were gavaged with 200 μL PBS; (2) SL-trained FEVs group (SL-FEVs), mice were gavaged with 50 μg SL-trained FEVs in 200 μL PBS (the dose corresponds to the total protein content of FEVs, quantified via the BCA method). The administration of SL-trained FEVs continued for an additional 5 days. The specific workflow was illustrated in Fig. 6A.

2.9 Intervention of miRNA-depleted SL-trained FEVs in ulcerative colitis mice

To prepare the miRNA-depleted SL-trained FEVs (de_miRNA) control, we employed a method combining ultrasonication and RNase treatment. The purified SL-trained FEVs suspension was subjected to ultrasonication on ice using a sonicator to completely disrupt the vesicles. Subsequently, RNase A was added to the lysate, followed by incubation at 37°C for 45 min.

Male C57BL/6J mice, weighing between 22 and 25 g, were sourced from Changzhou Cavens Lab Animal Co. After a 1-week adaptation period, 18 mice were randomly divided into two groups: The normal control group (Con), mice were given normal drinking water (n=6), and the DSS model group (DSS), mice were given 2.5% DSS drinking water (n=12). After 2 days, mice in the DSS group were further divided into 2 subgroups (n=6): (1) DSS model group (DSS), mice were gavaged with PBS; (2) de_miRNA SL-trained FEVs group (de_miRNA), mice were gavaged with 50 μg/day in 200 μL PBS. Drug administration continued for an additional 5 days.

2.10 The preventive effect of TCDCA in ulcerative colitis mice

After a 1-week adaptation period, 24 mice were randomly divided into two groups: The normal control group (Con), mice were given normal drinking water (n=6), and the DSS model group (DSS), mice were given 2.5% DSS drinking water (n=18). After 2 days, mice in the DSS group were further divided into 3 subgroups (n=6): (1) DSS model group (DSS), mice were gavaged with PBS; (2) TCDCA low dosage (TCDCA-L), mice were gavaged with 100 mg/kg TCDCA; (3) TCDCA high dosage (TCDCA-H), mice were gavaged with 200 mg/kg TCDCA. Drug administration continued for an additional 5 days.

2.11 Disease activity index (DAI) and colon histopathological analysis

DAI was assessed using the previously mentioned procedures to determine the severity of the colitis [21]. After drying, the colon tissues were promptly fixed in 4% paraformaldehyde, embedded in paraffin, and sectioned at a thickness of 5 μm. Tissue sections from each mouse group were stained with hematoxylin and eosin (H&E) and examined microscopically for histopathological analysis.

2.12 Determination of inflammatory factors

Blood collected from the mice's orbits was centrifuged at 10000 r/min for 15 min to separate the serum. The concentrations of TNF-α, IL-1β, IL-6, and IL-18 were then measured according to the instructions provided with the ELISA kit.

2.13 Western blots, immunohistochemistry, and immunofluorescence staining

Western blots, immunohistochemistry, or immunofluorescence staining were used to detect the expression of target proteins. In colonic tissues or sections, specific antibodies were employed to detect target proteins, followed by a combination of secondary antibodies. The bands from Western blots were captured using a Tanon 5200 imaging system, while tissue sections were digitized using a Pannoramic MIDI automatic slide scanner (3DHISTECH Ltd., Budapest, Hungary). Densitometric measurements were calculated with ImageJ software (version 7, NIH, USA).

2.14 Analysis of gut microbiota by 16S rRNA gene sequencing

At the end of the experimental period, faeces in the colon were collected from mice across all groups. The hypervariable V3-V4 region of the 16S rRNA gene was amplified. The raw sequencing data were processed using the Illumina HiSeq X Five platform. Sequencing services were provided by Hangzhou Lianchuang Biotechnology Co. (Hangzhou, China), and further analysis was performed using tools available on OmicStudio (https://www.omicstudio.cn/tool).

2.15 Bile acids (BAs) analysis

BAs concentrations in faeces contents samples were measured using a Thermo Fisher Scientific TSQ Altis triple quadrupole mass spectrometer with an ESI Turbo Ion-Spray interface and a Vanquish UPLC system. Hangzhou Lianchuang Biotechnology Co. (Hangzhou, China) conducted the analysis. A 50 mg sample was extracted with methanol/water and collected the supernatant for UPLC-MS/MS analysis. Chromatographic separation was performed on a Waters ACQUITY UPLC BEH C18 column (2.1 × 100 mm, 1.7 μm). The mobile phases were 0.1% formic acid (A) and isopropanol-acetonitrile (7:3) (B). The injection volume was 5 μL, the column temperature was 40°C, and the ESI-MS/MS operated in negative ion mode with multi-response monitoring (MRM). Key ESI parameters were: 400°C temperature, 4500 V spray voltage, 55 Arb sheath gas, and 10 Arb auxiliary gas.

2.16 Statistical analysis

Data are presented as mean ± SEM. Statistical analysis was conducted using either Student's t-test or one-way ANOVA. Significance levels were set at $P < 0.05$.

3. Results

3.1 Identification of SL in chicory leaves

By comparing the UV spectra of the standards and the samples, it was determined that the SL extracted from chicory leaves mainly contain seven different sesquiterpene lactones. The structures and retention times of these compounds are detailed in Fig. 1 and Table 1. The unidentified compounds 3 and 6 were preliminarily identified based on their characteristic UV absorption wavelengths and retention times, which are typical for sesquiterpene lactones. Their specific UV absorption spectra are provided in the Supplementary Files. Under the HPLC conditions established in Fig. 1, we calculated the ratio of the total peak area of all identified SL to the total peak area of all detectable components in the fraction. The results showed that the purity of the major

SL in the chicory concentrate fraction was 46.52%. The total SL yield per 100 g dry weight of leaves was 0.615 ± 0.14 g. Finally, the SL yield was determined to be 0.286 ± 0.07 mg/100 g dry weight (mean ± SD, n=3). [23]

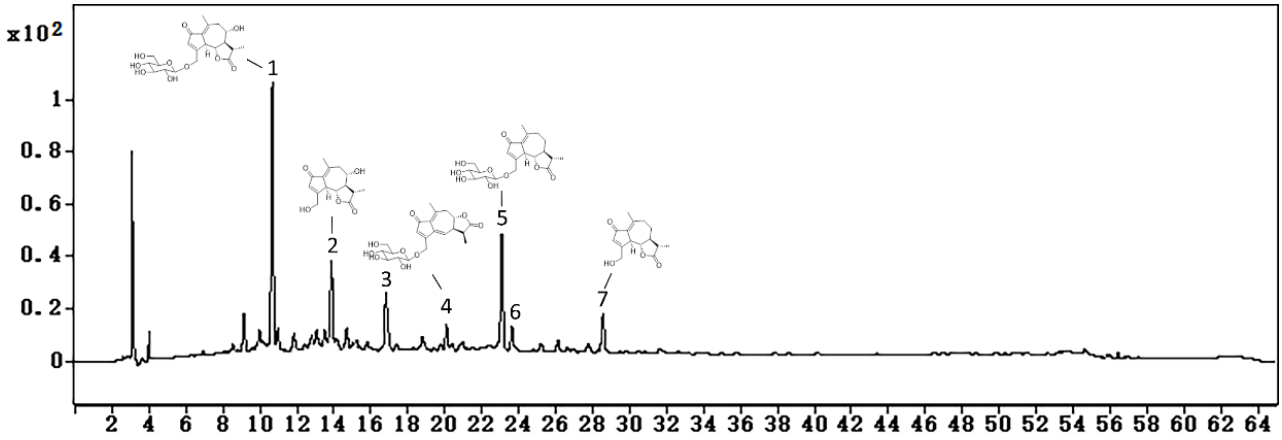

Figure 1. Sesquiterpene lactones (SL) were structurally identified from fresh chicory leaves.

Table 1. Information of total sesquiterpene lactones from fresh chicory leaves

No.	RT (min)	Compounds	Rel. area %
1	10.664	cichorioside B	15.57
2	13.858	11β, 13-Dihydrolactucin	9.52
3	17.062	unknown sesquiterpene lactones	6.67
4	20.084	Intybusin A	2.80
5	23.084	crepidiaside B	6.51
6	24.067	unknown sesquiterpene lactones	3.24
7	28.571	jacquilenin	2.21

3.2 Chicory SL administration alleviated symptoms in DSS-induced UC mice

DSS-induced UC mice were used to investigate whether SL could alleviate UC development. In Fig. 2B-E, it was shown that DSS significantly reduced body weight and colon length. DSS also significantly increased the DAI index. However, administration of SL, especially at a high dose, reversed these abnormalities. Furthermore, SL treatments significantly decreased the increase of TNF-α, IL-1β, IL-6, and IL-18 caused by DSS (Fig. 2F-I, $P < 0.05$).

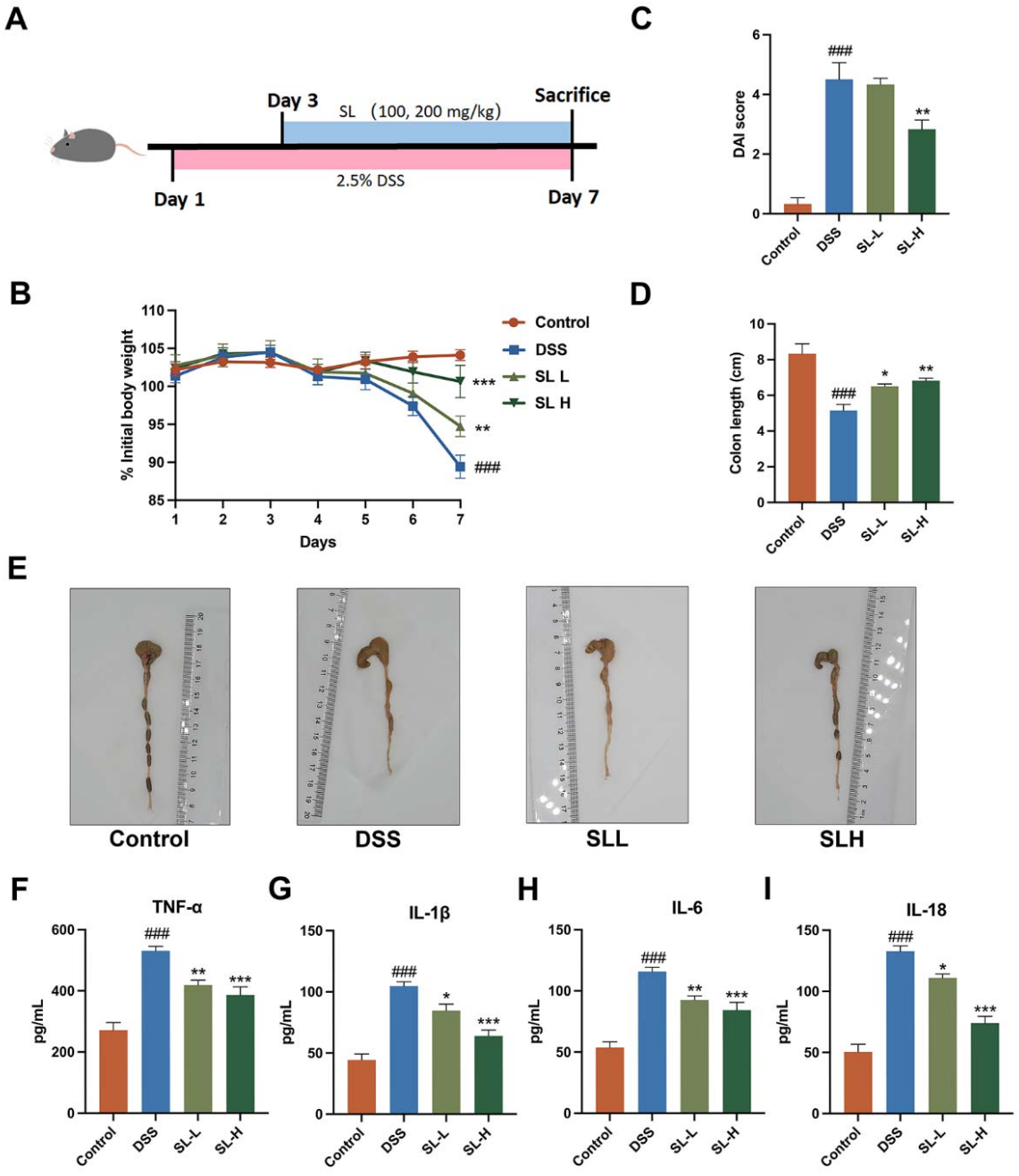

Figure 2. Chicory SL administration alleviated symptoms in DSS-induced UC mice. (A) Workflow chart. (B) Body weight changes in mice. (C) DAI scores. (D) Colon length measurements. (E) Representative images of colon length. (F-I) Levels of TNF-α, IL-1β, IL-6, and IL-18 in the serum (n=10). $^{###}P < 0.001$ vs. control group, $^{*}P < 0.05$, $^{**}P < 0.01$, and $^{***}P < 0.001$ vs. DSS group.

3.3 Chicory SL administration modulated intestinal injury and intestinal barrier

Pathological histological studies (H&E staining) demonstrated that DSS induced colonic barrier damage, characterized by crypt degeneration, depletion of goblet cells, and infiltration of inflammatory cells, while SL administration simultaneously reversed these symptoms (Fig. 3A). Additionally, we investigated the role of SL in modulating intestinal barrier proteins. The results indicated that DSS dramatically decreased the levels of tight junction proteins ZO-1, Occludin, Claudin-1, and the adhesion junction protein E-Cadherin, whereas SL therapy substantially increased the expression of these proteins (Fig. 3B-F).

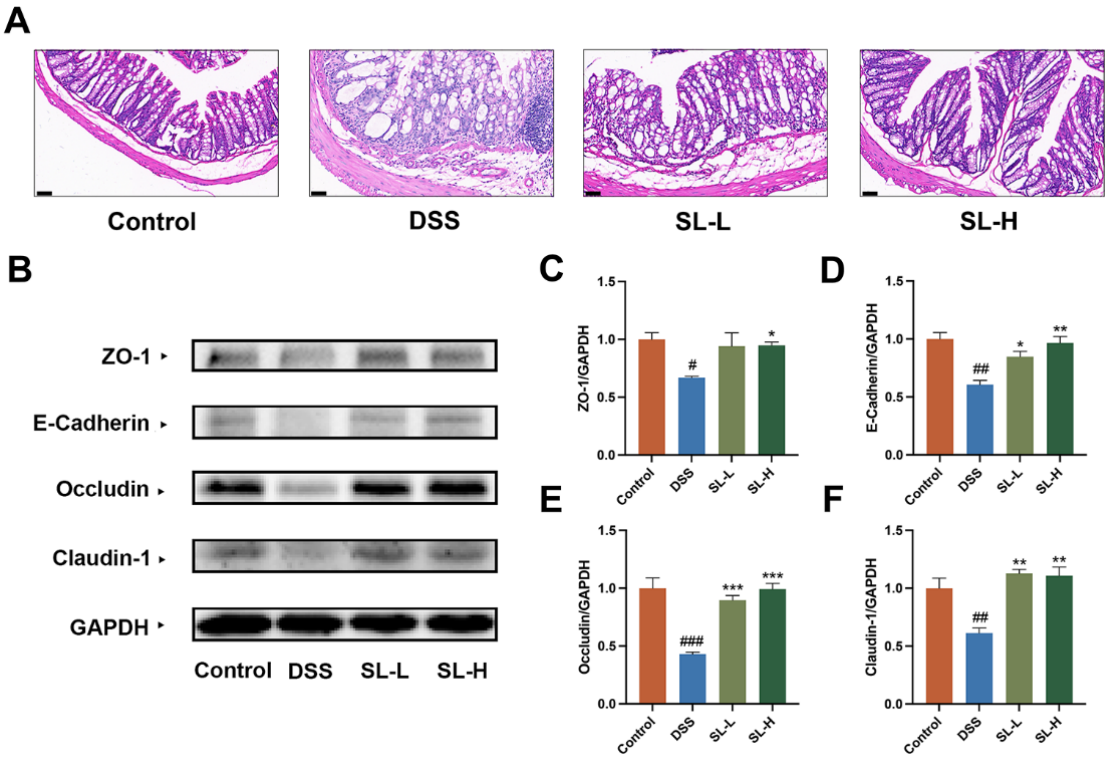

Figure 3. Chicory SL administration modulated intestinal injury and intestinal barrier. (A) H&E staining. (B) Representative bands of ZO-1, E-Cadherin, Occludin, and Claudin1. (C-F) Protein levels of ZO-1, E-Cadherin, Occludin and Claudin1. (n=3). $^{\#\#}P < 0.01$ and $^{\#\#\#}P < 0.001$ vs. control group, $^{*}P < 0.05$, $^{**}P < 0.01$, and $^{***}P < 0.001$ vs. DSS group.

3.4 Chicory SL administration mitigated DSS-induced gut microbiota dysbiosis

We performed 16S high-throughput sequencing to examine the effect of SL isolated from chicory on the gut microbiota. In Fig. 4A, principal coordinates analysis (PCoA) revealed distinct differences in gut microbiota between the control and DSS model groups. Following SL treatment, the gut microbiota exhibited a shift compared to the DSS group. DSS treatment at the phylum level led to an increased prevalence of Proteobacteria and Verrucomicrobiota, while Patescibacteria exhibited a decreased abundance. SL treatment partially restored the abundance of these gut microbiota (Fig. 4B). At the genus level, several vital taxa showed significant changes, including *Oscillibacter*, *Odoribacter*, *Candidatus Saccharimonas*, and *Escherichia-Shigella*. Specifically, SL significantly increased the abundance of *Odoribacter* and *Candidatus Saccharimonas* while substantially reducing the abundance of *Oscillibacter* and *Escherichia-Shigella*, compared to the DSS model group (Fig. 4C-F). The linear discriminant analysis effect size (LEfSe) analysis was performed to identify the most significant differences among the control, DSS, and SL-treated groups. At the genus level, *Prevotellaceae_UCG-001* and *Oscillibacter* were enriched in the DSS group, whereas *Lactobacillus* and *Ligilactobacillus* were more abundant in the control group. Following SL treatment, this pattern was reversed, with increased levels of *Clostridia_UCG014_unclassified*, *Alistipes*, *Anaerotipes*, and *Odoribacter spp* (Fig. 4G and H). These results suggest that SL has regulatory effects on gut microbiota composition. KEGG analysis revealed that bile acids metabolism, particularly pathways related to bile secretion, biosynthesis of secondary bile acids, and biosynthesis of primary bile acids, is a critical metabolic process influenced by gut microbiota in DSS-induced UC mice (Fig. 4I).

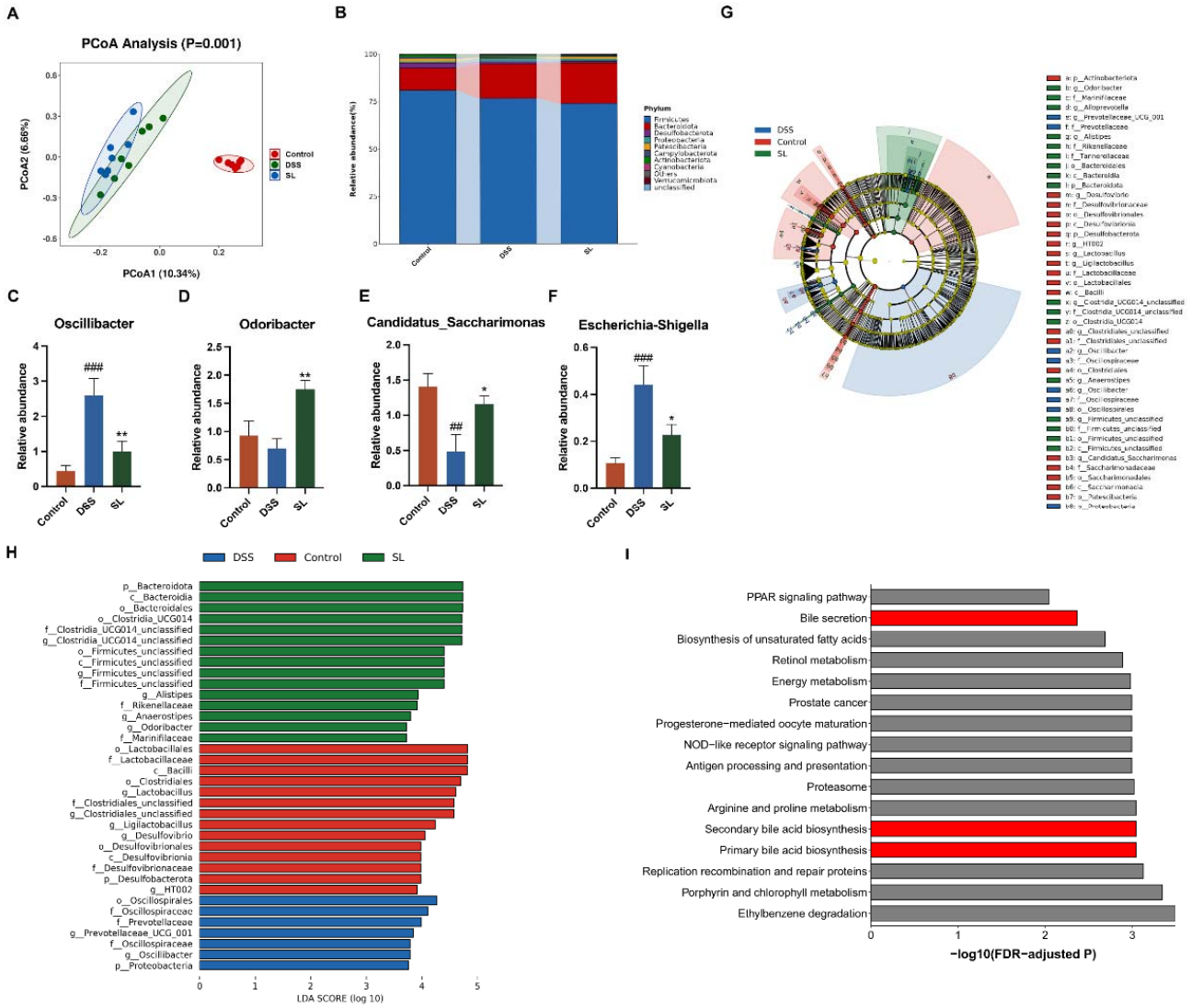

Figure 4. Chicory SL mitigated DSS-induced gut microbiota dysbiosis. (A) PCoA plot. (B) The microbiota characteristics at the phylum level. Relative abundance of (C) *Oscillibacter*, (D) *Odoribacter*, (E) *Candidatus Saccharimonas*, and (F) *Escherichia-Shigella*. LEfse analysis of (G) evolutionary branching diagram and (H) distribution histogram. (I) KEGG pathway prediction. $^{\#\#}P < 0.01$ and $^{\#\#\#}P < 0.001$ vs. control group, $^{*}P < 0.05$, and $^{**}P < 0.01$ vs. DSS group (n=8).

3.5 Chicory SL modulated BAs metabolism profiles in DSS-induced mice

Based on the KEGG results, we further analyzed the alterations in bile acids across different groups of mice. As shown in Fig. 5A, DSS treatment altered the BAs profile compared to the control group, while SL administration resulted in a distinct segregation of BAs components, indicating a different profile. As shown in Fig. 5B, DSS induced a reduction in total bile acids levels in the faeces, which was improved by SL treatment. Specifically, SL treatment significantly increased the primary bile acids taurocholic acid (TCA) and TCDCA, as well as the secondary bile acids tauroursodeoxycholic acid (TUDCA) and lithocholic acid (LCA), while significantly decreasing the levels of the secondary bile acid 23-nordeoxycholic acid (NorDCA) (Fig. 5C-G). Spearman's correlation analysis revealed that TCDCA were significantly positively correlated with *Lactobacillus*, *Ligilactobacillus* and *Candidatus_Saccharimonas*, and negatively correlated with

Oscillibacter and *Escherichia-Shigella*. *Lactobacillus* and *Ligilactobacillus* were negatively correlated with NorDCA. Additionally, *Candidatus_Saccharimonas* and *Ligilactobacillus* were significantly positively correlated with TCA and TUDCA, respectively (Fig. 5H, $P < 0.05$).

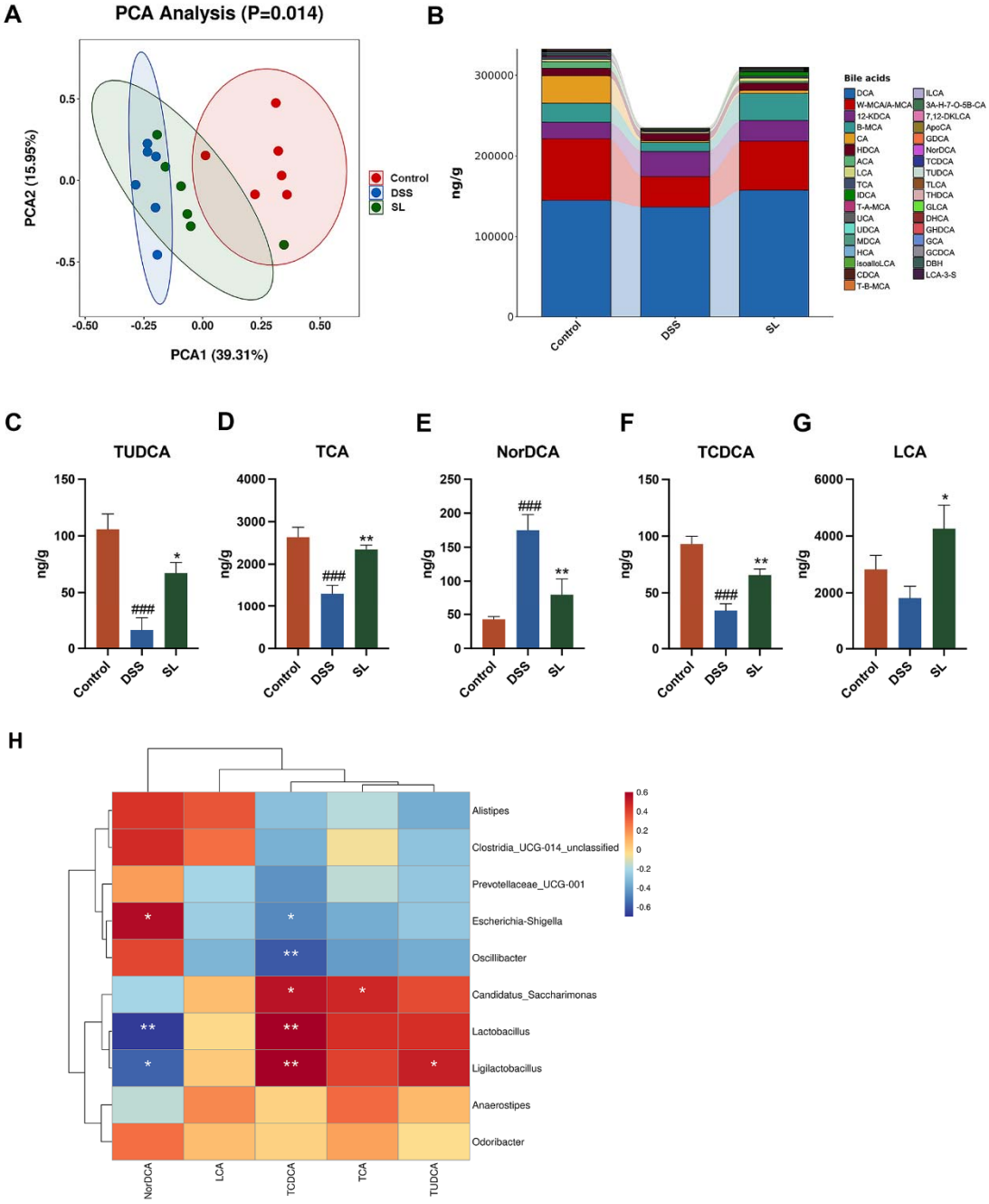

Figure 5. Effect of Chicory SL on bile acids metabolism in DSS-induced mice. (A) PCoA plot. (B) Total bile acids levels. (C-G) Differential bile acids contents (H) Association analysis of BAs with differential genera of gut microbiota. $^{###}P < 0.001$ vs. control group, $^{*}P < 0.05$, and $^{**}P < 0.01$ vs. DSS group (n=6).

3.6 Morphology characterization and miRNA profiling of chicory SL-trained FEVs

Colonic contents were collected, and FEVs were isolated through ultracentrifugation using sucrose gradients (Fig. 6A). FEVs were harvested from the 30-45% interface of the sucrose gradient. As depicted in Fig. 6B-D, these particles displayed an exosome-like morphology with intact membranes and an average diameter of 71.1 ± 11.3 nm, the particle concentration at about 2.5×10^9 particles/mL. Additionally, miRNA

profiling was performed to evaluate changes in FEVs across different treatment groups. The Venn diagram, heatmap, and volcano plot revealed significant differences in FEV-miRNA profiles among the control, DSS, and SL treated groups. Notably, several miRNAs with significant variations were identified, including miR-144-3p, miR-25-3p, miR-126a-5p, miR-26a-5p, and miR-215-5p (Fig. 6E-G). Gene Ontology (GO) enrichment analysis highlighted the top 10 enriched miRNAs in FEVs across different groups, which were related to processes such as signal transduction, G protein-coupled receptor signaling, and protein binding (Fig. 6H). Furthermore, Kyoto Encyclopedia of Genes and Genomes (KEGG) pathway analysis revealed that FEVs were also associated with critical signaling pathways, including adherens junctions, the Wnt signaling pathway, and bacterial invasion of epithelial cells (Fig. 6I).

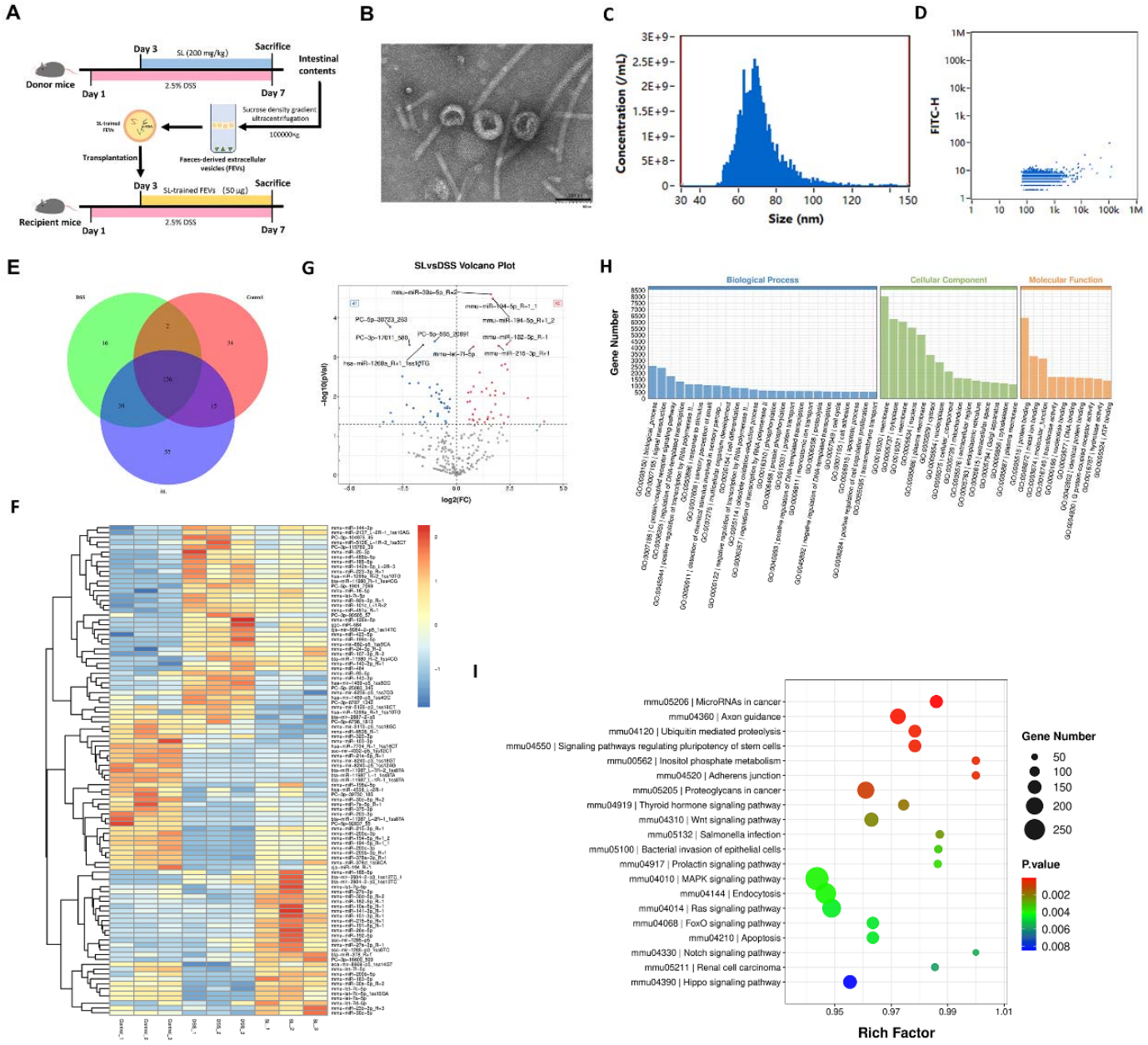

Figure 6. Isolation, characterization, and miRNA profiling of SL-trained FEVs. (A) Schematic representation of the isolation process for SL-trained FEVs. (B) Morphological characterization of FEVs using transmission electron microscopy (scale bar = 100 nm). (C, D) Nanoparticle tracking analysis of FEVs size distribution and concentration. (E-G) miRNA profiling analysis, including (E) Venn diagram, (F) heatmap, and (G) volcano plot comparisons between control, DSS, and SL groups. (H) GO and (I) KEGG pathway analysis of differentially expressed miRNAs in FEVs.

3.7 SL-trained FEVs transplantation alleviated symptoms in DSS-induced UC mice

After gavage, SL-trained FEVs were absorbed in the gastrointestinal tract within 24 h (Fig. 7A). DSS treatment significantly reduced the body weight of the mice compared to the control group, whereas SL-trained FEVs notably increased body weight ($P < 0.05$). Furthermore, SL-trained FEVs effectively reversed the DSS-induced increase in DAI scores (Fig. 7C, $P < 0.01$). Fig. 7D and E illustrate that DSS administration led to a reduction in colon length compared to the control group. However, this effect was significantly mitigated by SL-trained FEVs ($P < 0.05$). To assess the anti-inflammatory effects of SL-trained FEVs, serum inflammatory markers were measured. As shown in Fig. 7F-I, DSS treatment markedly increased the levels of TNF-α, IL-1β, IL-6, and IL-18, while SL-trained FEVs significantly reduced these inflammatory cytokines ($P < 0.001$). H&E staining revealed marked inflammatory infiltration and crypt distortion in the colonic tissue of the DSS group, whereas treatment with SL-trained FEVs alleviated these symptoms (Fig. 7J). In addition, we explored the effect of SL-trained FEVs on the expression of proteins such as Claudin1, TLR4, NLRP3, NFκB, and p-NFκB. Immunohistochemistry and immunofluorescence results demonstrated that DSS markedly upregulated the expression of TLR4, NLRP3, and p-NFκB while downregulating the expression of Claudin1. However, treatment with SL-trained FEVs effectively reversed these changes (Fig. 7K-R, $P < 0.05$)

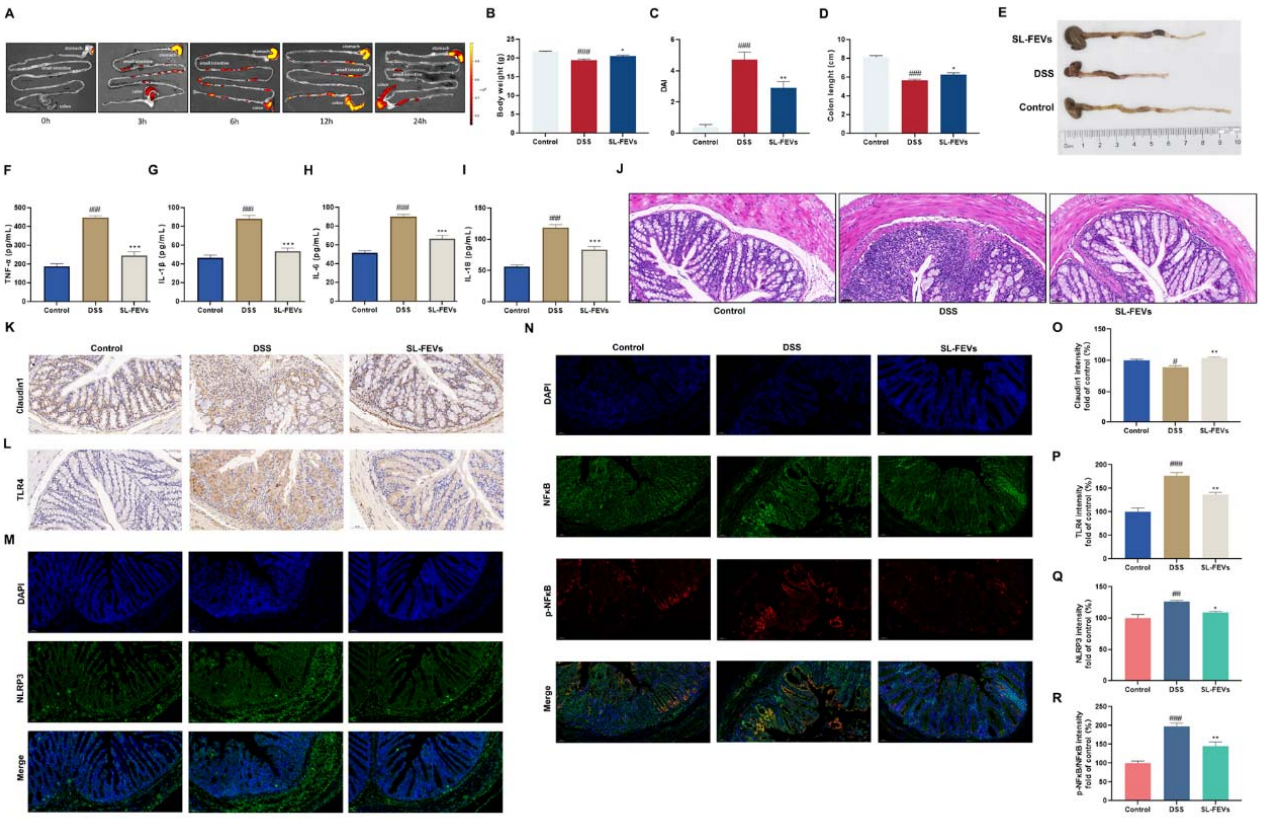

Figure 7. SL-trained FEVs transplantation ameliorated DSS-induced UC by attenuating intestinal injury, inflammation, and barrier dysfunction. (A) Fluorescence images of the intestinal tract at 0, 3, 6, 12, and 24 h after receiving SL-trained FEVs. (B) Body weight changes in mice. (C) DAI scores. (D) Colon length. (E) Representative images of colon length. Levels of (F) TNF-α, (G) IL-1β, (H) IL-6, and (I) IL-18 in the serum of mice (n=10). (J) H&E staining. Immunohistochemical staining of (K) Claudin1 and (L) TLR4 in colon tissue. Immunofluorescence staining of (M) NLRP3, (N) NFκB, and p-NFκB in colon tissue. (O-R) Analysis of the positive area of Claudin1, NLRP3, NFκB, and p-NFκB (n=3). Scale bar = 50 μm. $^{\#\#\#}P < 0.001$ vs. control group, $^{*}P < 0.05$, $^{**}P < 0.01$, and $^{***}P < 0.001$ vs. DSS group.

3.8 SL-trained FEVs transplantation mitigated DSS-induced gut microbiota dysbiosis

A Venn diagram illustrating the OTU levels of gut microbiota showed that the DSS group had the fewest OTUs. In contrast, the SL-trained FEVs transplantation group displayed a similar number of OTUs compared to the CON group (Fig. 8A). Chao1, Shannon, and Simpson index were used to describe the α-diversity of gut microbiota among the control, DSS and SL-trained FEVs group. The results showed that SL-trained FEVs improved the tendency of Chao1, Shannon, and Simpson to decrease (Fig. 8B-D, $P < 0.05$). PCoA analysis revealed that SL-trained FEVs significantly modulated the gut microbiota structure, distinct from the control and DSS groups (Fig. 8E). At the phylum level, the gut microbiota was predominantly characterized by p-Firmicutes, p-Bacteroidota, p-Desulfobacterota, p-Verrucomicrobiota, p-Proteobacteria, p-Cyanobacteria, and p-Actinobacteriota in the control group. Conversely, it was dominated by p-Firmicutes, p-Verrucomicrobiota, and p-Bacteroidota in the DSS group. At the genus level in the DSS group, and the most abundant gut microbiota (TOP 5) were *g-Lachnospiraceae_NK4A136_group*, *g-Akkermansia*, *g-Clostridium*, *g-Eubacterium_siraeum_group*, and *g-Alistipes* (Fig. 8F-H). DSS treatment significantly reduced the abundance of p-Bacteroidota and p-Patescibacteria while increasing the F/B ratio compared to the control group. Transplantation of SL-trained FEVs markedly increased the levels of p-Actinobacteriota and p-Patescibacteria (Fig. 8I-L, $P < 0.05$). Although not statistically significant, SL-trained FEVs also impacted p-Bacteroidota abundance and the F/B ratio (Fig. 8 I and J). LEfSe analysis was performed to further evaluate the variability and enrichment of gut microbial species from the phylum to species level (LDA score > 4, Fig. 8 M and N). In the control group, 18 taxa were found to be enriched, including p-Bacteroidetes, *g-Lachnospiraceae_unclassified,* o-Lactobacillales, *g-Alistipes, and g-Alloprevotella.* In contrast, the DSS group was predominantly characterized by p-Verrucomicrobiota, *g-Akkermansia*, and *g-Eubacterium_siraeum_group*. Notably, SL-trained FEVs transplantation significantly enriched *g-Clostridia_UCG014_unclassified*. These results indicate substantial alterations in gut microbial taxa across the control, DSS treatment, and SL-trained FEVs transplantation groups.

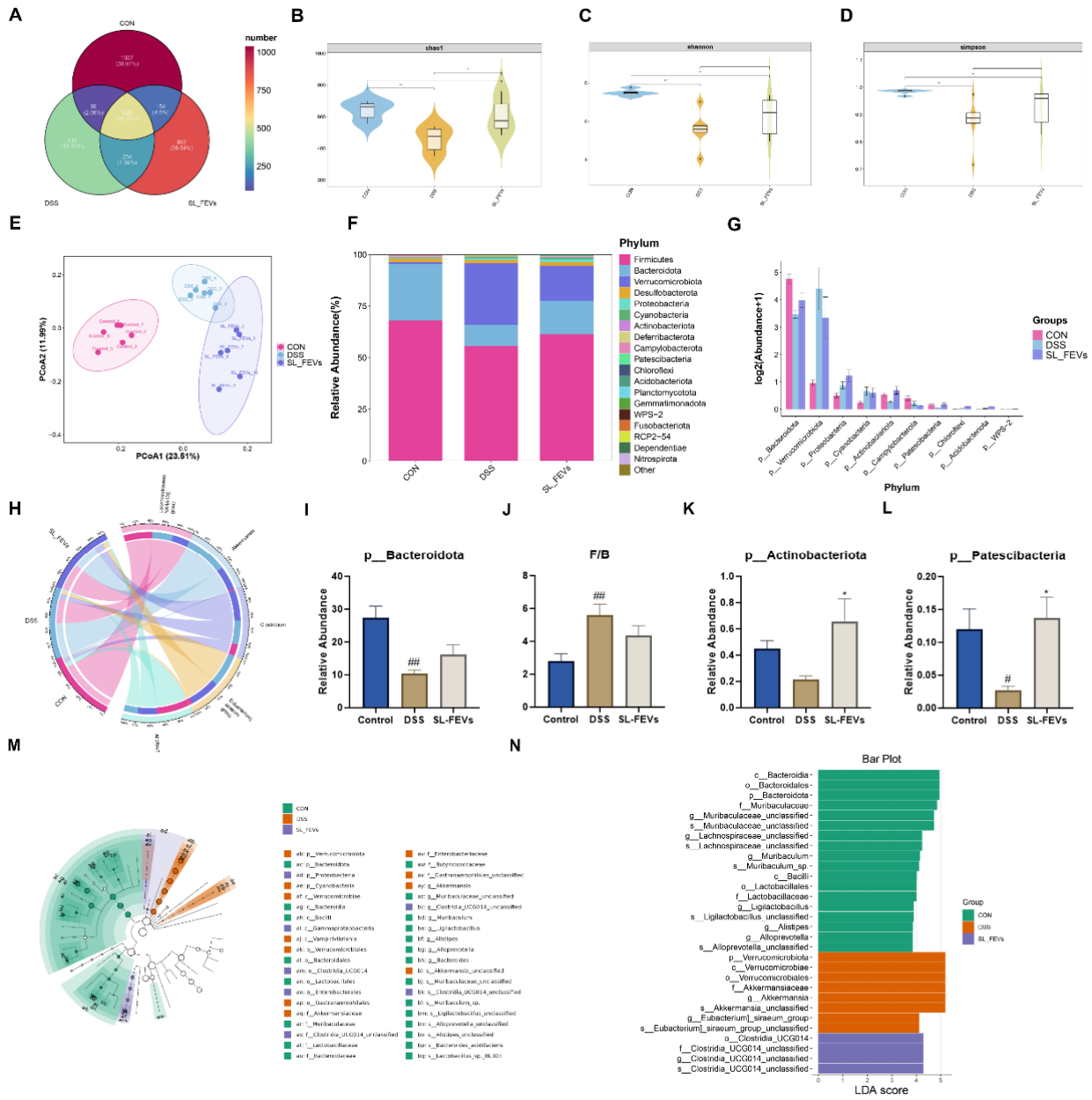

Figure 8. SL-trained FEVs transplantation mitigated DSS-induced gut microbiota dysbiosis. (A) Venn diagram. (B) Chao1, (C) Shannon, and (D) Simpson index. (E) PCoA index. (F) Relative abundance of major microbiota at the phylum level. (G) Top 10 microbiota characteristics at the phylum level and (H) Top 5 microbiota characteristics at the genus level. Relative abundance of (I) Bacteroidota, (J) F/B ratio, (K) Actinobacteriota, and (L) Patescibacteria at the phylum level. (M) Evolutionary branching plot and (N) distribution histogram of LEfSe analysis. $^{\#}P < 0.05$, and $^{\#\#}P < 0.01$ vs. control group, $^{*}P < 0.05$, and $^{**}P < 0.01$ vs. DSS group (n=6).

3.9 SL-trained FEVs transplantation modulated DSS-induced BAs metabolism profiles

Since BAs are essential for maintaining intestinal homeostasis, we examined the effects of SL-trained FEVs transplantation on BAs levels in DSS-induced mice. As illustrated in Fig. 9A, the PCA plot shows distinct BAs profiles across different groups. A total of 35 distinct BAs were identified among the control, DSS, and SL-trained FEVs administration groups. DSS treatment reduced total intestinal BAs levels, a reduction that was improved by SL-trained FEVs transplantation (Fig. 9B). In DSS-treated mice, levels of the primary bile acids tauro-α-muricholic acid (T_α_MCA), tauro-β-muricholic acid (T_β_MCA), TCA, and TCDCA, along with the secondary bile acid LCA, were markedly decreased (Fig. 8C-I, $P < 0.05$), while

NorDCA, another secondary bile acid, showed an increase. These changes were reversed by SL-trained FEVs transplantation. Fig. 9J showed that Spearman's correlation analysis identified a significant positive association between p-Actinobacteriota and LCA, while NorDCA was negatively associated with p-Actinobacteriota. Additionally, *g-Clostridium* was negatively correlated with levels of LCA, TCA, T_α_MCA and T_β_MCA ($P < 0.05$). Furthermore, p-Patescibacteria was significantly positively correlated with LCA and negatively correlated with NorDCA ($P < 0.05$).

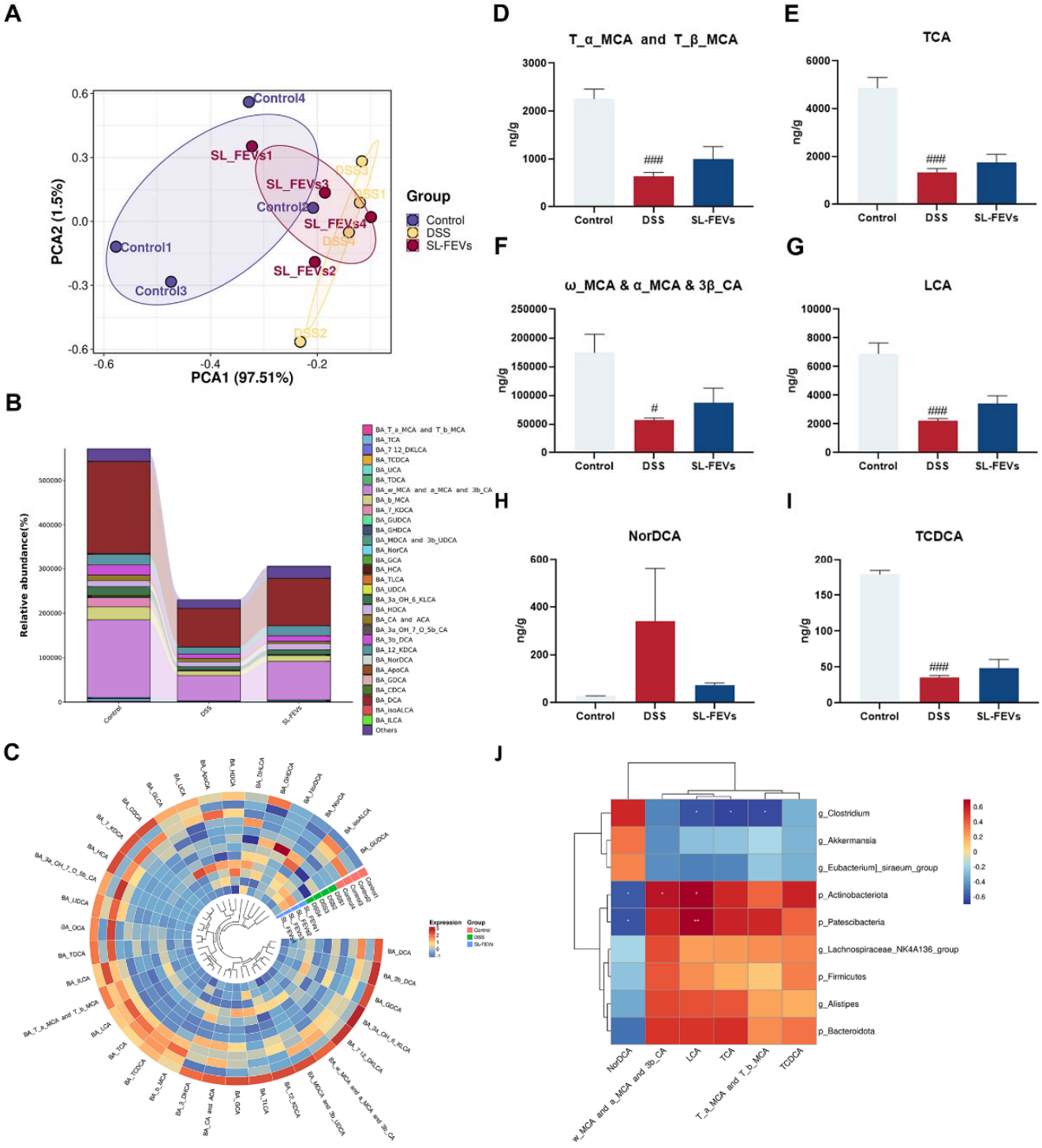

Figure 9. Effect of SL-trained FEVs transplantation on bile acids metabolism in DSS-induced mice. (A) PCoA plot. (B) Total bile acids levels. (C) Heatmap. (D-I) Differential bile acids contents (J) Association analysis of BAs with differential gut microbiota. $^{\#}P < 0.05$, $^{\#\#\#}P < 0.001$ vs. control group. $^{*}P < 0.05$, $^{**}P <$ 0.01 (n = 4).

3.10 Intervention of miRNA-depleted SL-trained FEVs in ulcerative colitis mice

The therapeutic efficacy of SL-trained FEV-s was significantly attenuated by the depletion of miRNAs. Compared to the untreated SL-trained FEVs group, the body weight of mice in the de_miRNA FEVs treatment group showed no significant improvement, with a declining trend similar to the DSS model group (Fig. 10B). Meanwhile, de_miRNA FEVs also failed to effectively alleviate DSS-induced colon shortening, showing no statistical difference in colon length compared to the DSS group. (Fig. 10C and E) Regarding the DAI score, the de_miRNA FEVs group maintained a consistently high level (Fig. 10F).

At the histopathological level, H&E staining showed that colon tissue from mice treated with de_miRNA FEVs still exhibited significant inflammatory cell infiltration, crypt destruction, and loss of epithelial integrity, with pathological damage comparable to the DSS group (Fig. 10D). Further ELISA detection revealed that serum levels of key pro-inflammatory cytokines, including TNF-α, IL-1β, IL-6, and IL-18 (Fig. 10G-J), remained high in this group, showing no significant decrease compared to the DSS model group, indicating an inability to effectively control the clinical severity of the disease.

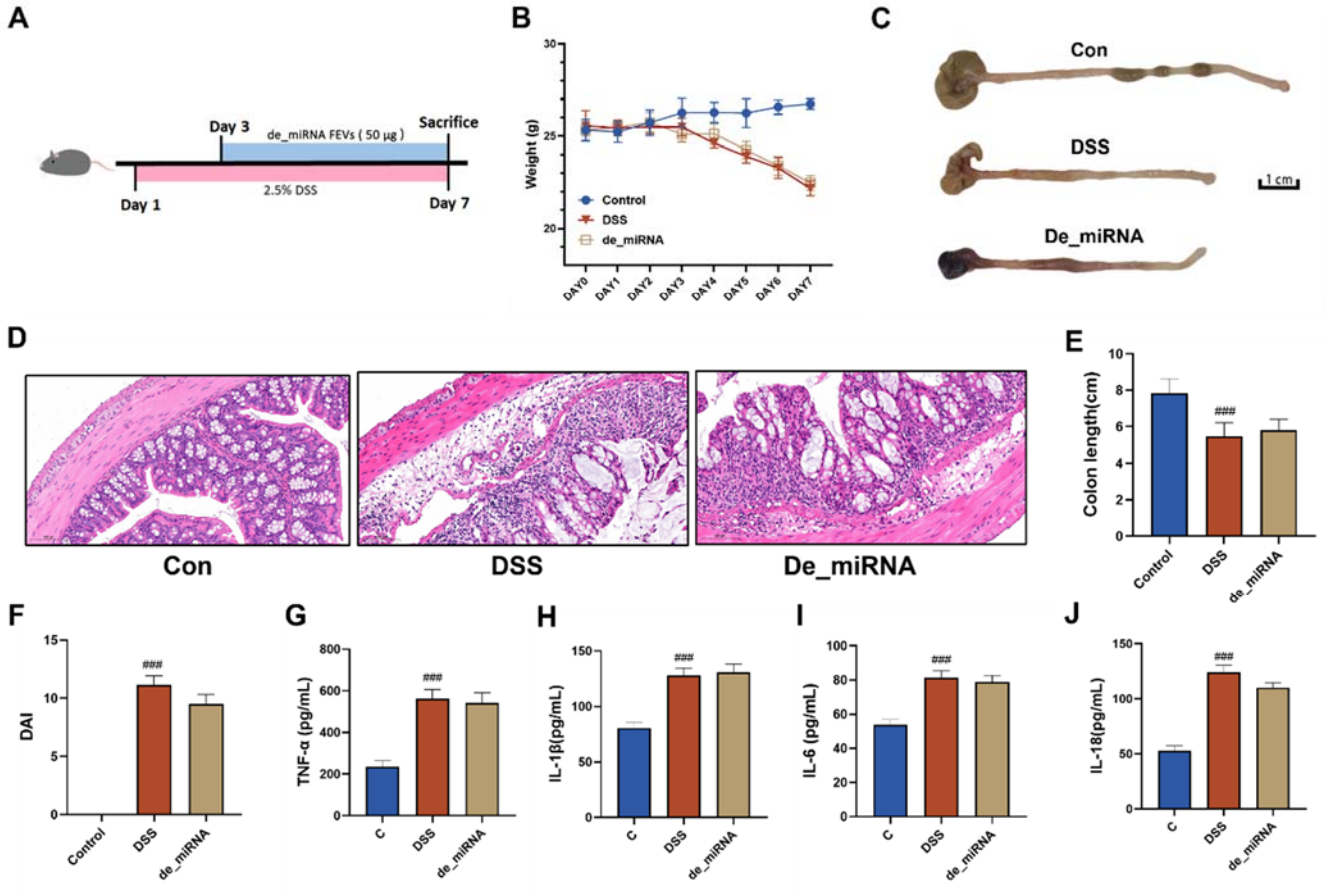

Figure 10. The therapeutic efficacy of SL-trained FEVs was significantly attenuated by the depletion of miRNAs. (A) Schematic diagram of the experimental design. (B) Body weight changes in mice. (C) Representative images of colon length. (D) H&E staining of colon tissues. (E) Colon length measurements. (F) DAI scores. Levels of (G) TNF-α, (H) IL-6, (I) IL-1β, and (J) IL-18 in the serum of mice (n=6). $^{###}P < 0.001$ vs. control group.

3.11 TCDCA alleviated symptoms in DSS-induced UC mice

To investigate the role of bile acids in DSS-induced UC, we administered TCDCA as an interventional agent (Fig. 11A). TCDCA treatment restored body weight and colon length in UC mice to levels comparable

to those in the Control group (Fig. 11B-D). It also significantly reduced the DAI elevated by DSS (Fig. 11E). Histological analysis via H&E staining further revealed that TCDCA ameliorated DSS-induced colonic damage, including crypt degeneration and inflammatory cell infiltration (Fig. 11F). Moreover, while DSS increased the levels of pro-inflammatory cytokines (TNF-α, IL-6, IL-1β, and IL-18), TCDCA intervention markedly lowered these inflammatory markers (Fig. 11G-J). Notably, the protective effects of TCDCA against UC exhibited a discernible dose-dependent trend.

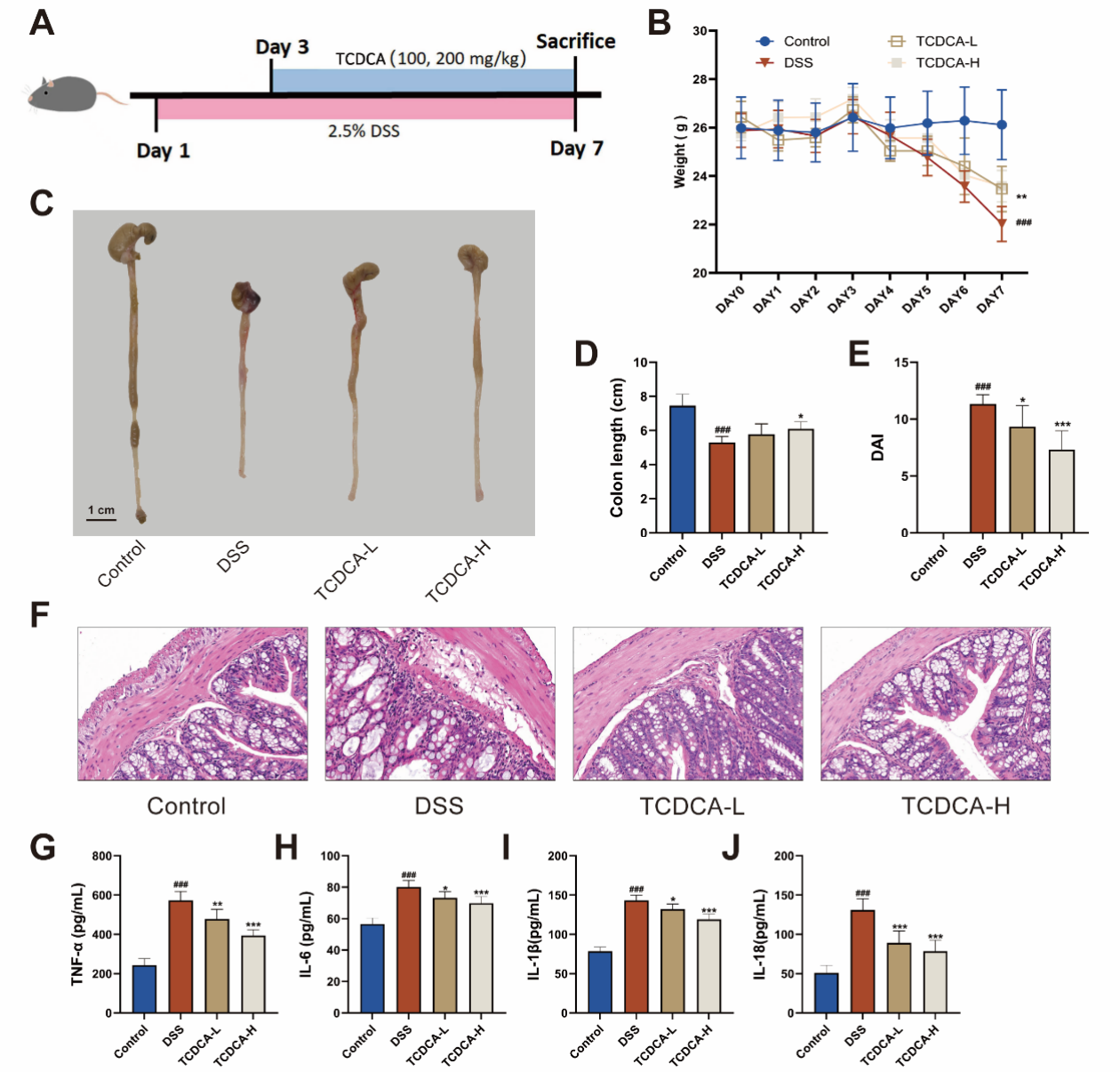

Figure 11. Intervention with TCDCA ameliorated DSS-induced ulcerative colitis. (A) Schematic diagram of the experimental design. (B) Body weight changes in mice. (C) Colon length measurements. (D) Representative images of colon length. (E) DAI scores. (F) H&E staining of colon tissues. Levels of (G) TNF-α, (H) IL-6, (I) IL-1β, and (J) IL-18 in the serum of mice (n=6). $^{###}P < 0.001$ vs. Control group; * $P < 0.05$, ** $P < 0.01$, and *** $P < 0.001$ vs. DSS group.

4. Discussion

Dysbiosis of the gut microbiota was considered strongly associated with UC, and reshaping the microbial composition was recognized as a crucial therapeutic strategy for UC treatment [24]. Chicory, a widely consumed edible plant with numerous physiological benefits, has a correlation with its potential influence on

gut microbiota [21, 25]. This work focused on extracting a specific class of bioactive compounds of chicory, sesquiterpene lactones , and clarifying their functions in reducing inflammation, repairing the intestinal barrier, and alleviating intestinal damage in DSS-induced ulcerative colitis mice. Additionally, we also explored the mechanism of SL modulating gut microbiota and bile acids metabolism in UC mice. Notably, as mediators, EVs play a critical role in communication between the gut microbiota and the host. Furthermore, SL-trained faeces-derived extracellular vesicles (FEVs) were transplanted into DSS-induced UC mice to investigate their protected effects on UC symptoms, gut microbiota dysbiosis, and bile acids metabolism disorder.

Studies demonstrated that modulating the gut microbiota composition was an effective strategy for UC treatment [7]. Dietary plant compounds, including terpenes, show promise in UC treatment [26-29]. Chicory is a rich source of SL with anti-inflammatory activity [30, 31], but their effect on UC was unknown. To our knowledge, this is the first study to explore the therapeutic effect of chicory-originated SL in UC. In this study we isolated chicory SL and elucidated the composition firstly [31, 32]. Then, the mice treated with 2.5% DSS for 7 days were employed to assess the possible effects of SL derived from chicory. Our results showed that the DSS-induced UC model exhibited significant colonic shortening, weight loss, and an increase in inflammatory cytokines (TNF-α, IL-1β, IL-6, and IL-18), with pathological analysis confirming crypt loss and inflammatory cell infiltration, consistent with previous studies. Moreover, DSS-induced loss of tight junction proteins can compromise intestinal barrier function and increase intestinal permeability, potentially facilitating the translocation of inflammatory cytokines and gut microbiota into the circulatory system, which further worsens UC symptoms [33, 34]. SL administration markedly alleviated the symptoms as mentioned above. While this study demonstrates the therapeutic potential of SL, its dose–response design presents a limitation. The two selected doses (100 mg/kg and 200 mg/kg) were based on preliminary experiments and showed clear dose-dependent effects; however, the inclusion of an intermediate dose would have allowed for a more refined dose–effect relationship. Due to experimental constraints at the time, future studies will incorporate an intermediate dose to better define the optimal therapeutic window.

Fecal microbiota transplantation was considered as a therapeutic approach for UC, which highlighted the essential function of gut microbiota in the development and management of disease [35]. EVs are nanoscale particles secreted by mammals, bacteria, and plants, which play a crucial role in facilitating communication across species and kingdoms [36]. Studies suggest that faeces are rich in EVs, known as faeces-derived EVs (FEVs), which carry a variety of small biological molecules, particularly nucleic acids, and have been shown to influence host physiological processes, including impairing spermatogenesis and contribute to liver disease in mammals [13, 37]. Numerous studies have demonstrated that transplantation of FEVs derived from trained gut microbiota can alleviate various diseases, including intestinal disorders and UC [17, 38-40]. In the present study, we have demonstrated the therapeutic effect of SL on UC, and we further isolated FEVs from mouse colonic contents after SL training. Morphological analysis revealed that SL-trained FEVs were nanoscale particles (71.1 ± 11.3 nm) enriched in miRNAs. Subsequently, the therapeutic efficacy of these miRNA-enriched

SL-trained FEVs was evaluated in DSS-induced UC mice models. The results demonstrated that SL-trained FEVs successfully replicated the therapeutic efficacy of SL in UC treatment, showing marked anti-inflammatory activity and significant attenuation of intestinal injury. Our findings confirm that SL-trained FEV transplantation is a promising therapeutic strategy for UC.

Diet plays a pivotal role in shaping the composition of gut microbiota. Studies demonstrated that supplementation with plant-derived components could effectively modulate DSS-induced gut microbiota dysbiosis, therefore mitigating symptoms of UC [7]. *Oscillibacter* and *Escherichia-Shigella*, which were known as potential pathogenic bacteria, were observed significant increase in DSS-induced mice [41, 42]. In contrast, an increase in *Odoribacter* and *Candidatus Saccharimonas* abundance was associated with protective effects against DSS treatment [43, 44]. SL administration markedly reversed these abnormal patterns, modified gut microbiota composition in DSS-treated mice, consisted with previous investigations. Meanwhile, transplantation of SL-trained FEVs also led to significant alterations in gut microbiota composition in UC mice. Chlorogenic acid and riboflavin supplementation had been demonstrated to elevate Actinobacteriota levels and mitigate intestinal inflammation in DSS-treated mice [45, 46]. Notably, supplementation with plant extracts trained fecal gut microbiota markedly elevated Actinobacteriota levels, and showed therapeutic effects of UC [47]. H Gu et al. [48] demonstrated that administering plant extracts increased Patescibacteria levels, which were inversely correlated with serum levels of inflammatory factors, including TNF-α, IL-1β, IL-6, and IL-18, in DSS-treated mice. Our data suggested that transplantation of SL-trained FEVs influenced the mentioned gut microbiota to protect against DSS-induced intestinal damage and inflammation.

Diet not only altered the composition of the gut microbiota but also directly influenced the carriers of secretory EVs, including modifying the miRNA contents, which in turn impacted the cellular function of the host [49-51]. The FEVs-mediated pathway has gained increasing attention as a potential mechanism underlying diet-gut microbiota-host interactions [52]. After oral administration of SL, SL-trained FEVs exhibited distinct miRNA profiles compared to the control and DSS model groups, as revealed by Venn diagram analysis. miR-144-3p, miR-25-3p, miR-126a-5p, miR-200b-3p, and miR-26a-5p were significantly changed in SL-trained FEVs compared with DSS group. It has been shown that the increase in miR-144-3p in EVs had promoted inflammation and cellular fibrosis [53]. miR-25-3p had been shown to target TLR4, NLRP3, and NFκB, while FEVs had regulated the host inflammatory response through TLR4 mediation. Additionally, FEVs had also been demonstrated to influence tight junction proteins in intestinal epithelial cells, and these results were consistent with our immunofluorescence findings [14, 54, 55]. Levels of miR-26a-5p and miR-200b-3p in FEVs dramatically elevated from acute to remission phases in chronic colitis [56], while SL-trained FEVs were more abundant in miR-26a-5p and miR-200b-3p compared to DSS-trained FEVs, which exhibited alleviation in UC. Nanoparticles carrying miR-194-5p targeted the TLR4/NLRP3 signaling pathway to decrease the release of inflammatory substances during acute lung injury, while also altering tight junction proteins ZO-1 and Occludin to enhance vascular endothelial cell permeability and alleviate tissue

damage [57], and SL-trained FEVs regulated these targets for therapeutic benefits, possibly via increased miR-194-5p expression. Our data revealed that SL-trained FEVs enriched with miRNA effectively alleviated intestinal damage, restored intestinal barrier function, and inhibited inflammatory responses, primarily by regulating tight junctions and the TLR4/NLRP3/NFκB signaling pathway.

In addition to FEVs, BAs (metabolites of gut microbiota) are also involved in gut microbiota-host interactions. Studies have shown that gut microbiota-induced dysregulation of BAs metabolism plays an important role in the pathogenesis of UC [24]. Our data suggest that SL treatment altered the BAs profiles and attenuated the adverse symptoms in UC mice compared with normal mice. By comparing the levels of BAs in each group, TUDCA, TCA, NorDCA, TCDCA, and LCA were identified as differential BAs. Furthermore, the SL-trained FEV-treated group replicated SL's modulation of BAs, showing similar effects to SL. TUDCA exhibited anti-inflammatory effects and could promote the production of type 2 anion exchange protein (AE2), protecting cells from the harmful effects of toxic bile acids [58, 59]. Similarly, TCDCA, an important active component of BAs, demonstrated anti-inflammatory and immunomodulatory effects via interactions with the NFκB and AC-cAMP-PKA signaling pathways [60, 61]. The current investigation demonstrated that DSS markedly reduced TCDCA levels, while the administration of SL and SL-trained FEVs could modulate TCDCA. Decreased levels of LCA were observed under UC conditions, whereas increased LCA levels were shown to reduce inflammation in a colitis model [62, 63]. Our data corresponded with those reported in the literature. The correlation analysis revealed that the alterations in BAs caused by SL and SL-trained FEVs treatments were associated with *g-Clostridium* and *g-Alistipes*. Interestingly, EVs derived from Clostridium butyricum (an important member of the *g-Clostridium*) could influence the gut microbiota and bacterial metabolites to alleviate DSS-induced UC [64]. Clostridium butyricum-derived EVs had also been shown to restore miR-199a-3p expression, which could affect host functions, including inhibiting the NLRP3/caspase and NFκB signaling pathways, as well as restoring tight junction Claudin1 [65]. Additionally, Park et al [66]. demonstrated significant differences in the gut microbiota composition and diversity of FEVs between intestinal tumor patients and healthy individuals. Notably, EVs derived from the gut microbiota Alistipes were closely associated with the progression of intestinal tumors. The findings of our investigation indicated that by modulating the gut microbiota and altering microbiota-derived EVs in the faeces (including their miRNA cargo), SL alleviated DSS-induced UC, by improving BAs metabolism and regulating NLRP3/NFκB signaling pathways as well as tight junction proteins.

Beyond their well-documented roles in modulating inflammatory signaling and barrier integrity, the miRNAs enriched within SL-trained FEVs may also serve as direct or indirect regulators of bile acid metabolism-a possibility that remains largely unexplored in the context of microbiota-derived vesicles. Emerging evidence indicates that specific miRNAs can fine-tune the synthesis, transport, and signaling of bile acids by targeting key hepatic and intestinal genes. For instance, hepatic miR-34a has been shown to suppress CYP7A1, the rate-limiting enzyme in bile acid synthesis, while intestinal miR-144 can modulate the farnesoid X receptor (FXR) signaling pathway, a central regulator of bile acid homeostasis [67, 68]. This raises the

intriguing possibility that the SL-trained FEVs, upon intestinal delivery, may not only alleviate inflammation but also directly contribute to the normalization of the bile acid pool observed in our experiments-for example, the elevation of TCDCA and LCA-through their miRNA cargo. Thus, the miRNA profiling of FEVs, as conducted in this study, provides a crucial mechanistic link: it suggests that dietary components like SL can"program" the gut microbiota to release vesicles carrying specific regulatory miRNAs, which in turn may participate in restoring bile acid metabolism and, consequently, gut microbiota equilibrium. This proposed"miRNA-bile acid" axis adds a novel dimension to our understanding of how trained FEVs exert their therapeutic effects and warrants further functional validation in future studies. However, while we propose that the miRNA cargo of SL-trained FEVs may influence bile acid metabolism, the precise molecular mechanisms-specifically, which individual miRNAs target which key genes in the hepatic or intestinal bile acid synthesis, transport, or signaling pathways-remain to be definitively elucidated. Future studies employing gain- and loss-of-function approaches for specific miRNAs, combined with target gene validation, are warranted to causally link individual FEVs-derived miRNAs to the regulation of specific bile acid species and their downstream effects in UC.

A key question arising from our study concerns the comparative efficacy of direct SL administration versus SL-trained FEVs in reshaping gut microbiota and bile acid metabolism. While both interventions exerted substantial therapeutic effects on colitis symptoms and gut barrier function, nuanced differences were observed in their respective impacts on microbial diversity and BAs profiles. Specifically, although SL-trained FEVs recapitulated many of the microbial modulations seen with SL-such as enriching beneficial taxa like *Clostridia UCG014 unclassified* and *Alistipes*-their influence on certain bile acid species was less pronounced. For instance, both treatments consistently elevated levels of TCA, TCDCA, and LCA while suppressing NorDCA; however, these changes did not always reach statistical significance in the FEV-treated group. We propose several non-mutually exclusive explanations for this observed discrepancy. First, bile acid metabolism involves a highly complex regulatory network encompassing host enzymatic activities, gut microbial biotransformation, and nuclear receptor signaling. While SL compounds may directly and broadly influence multiple nodes within this network, FEVs-acting as natural nanocarriers-might exert more targeted and potentially delayed effects, possibly through the delivery of specific miRNA cargo. Second, the relatively modest and non-significant shifts in certain BAs following FEV treatment may reflect kinetic hysteresis, wherein the full normalization of BAs metabolism requires a longer intervention period than that required for amelioration of inflammation or epithelial repair. Third, it is plausible that the dosage or duration of FEV administration used here, though sufficient to alleviate colitis, was inadequate to fully restructure the BAs pool. To functionally validate the role of bile acids in the SL-FEV axis and bridge the observed gap between the two interventions, we performed supplementary experiments using TCDCA-a primary bile acid consistently modulated by both SL and SL-trained FEVs. Remarkably, TCDCA supplementation alone significantly attenuated colitis severity, restored intestinal barrier integrity, and suppressed pro-inflammatory signaling, thereby recapitulating key therapeutic benefits common to both SL and SL-trained FEV treatments.

This not only confirms TCDCA as a functional mediator shared by the two interventional strategies but also provides mechanistic support for the notion that FEVs act, at least in part, through fine-tuning host–microbiota crosstalk in BAs metabolism.

5. Conclusion

In summary, SL isolated from medicinal and edible plant Chicory trained FEVs, which had different miRNA compared with those from DSS-induced UC mice. SL-trained FEVs replicated the therapeutic effects of SL on UC, including anti-inflammatory effects, restoration of intestinal barrier function, and attenuation of intestinal damage. The potential mechanism of the effects on UC probably involved modulating gut microbiota, bile acids metabolism, and the NLRP3/NFκB signaling pathway. These findings not only illustrate the mechanisms by which diet changes gut microbiota and how FEVs subsequently modulate host function but also propose a potential treatment for UC utilizing SL and SL-trained FEVs.

Acknowledgments

We thank Mrs. Kai Tie for providing literature collation and analysis. The Jiangsu Provincial Service Center for Antidiabetic Drug Screening, named the Jiangsu Scientific and Technological Innovations Platform, also provided support. We are grateful for bioinformatics support from LC-Bio Co., Ltd (Hangzhou, China).

Funding

This study was supported by grants from the National Natural Science Foundation of China (32570442, 32100253, 81973463, 32170377) and the Open Fund of Jiangsu Key Laboratory for the Research and Utilization of Plant Resources (document number JSPKLB202315, JSPKLB202201).

Ethics approval and consent to participate

The animal studies were approved by the Animal Ethics Committee of China Pharmaceutical University (No. 2023-03-004).

Data availability statement

All data are available in the main text. The data are available from the corresponding author on reasonable request. The original datasets for the miRNA sequencing and bile acid metabolomics analyses have been deposited on Mendeley Data and are accessible via the following DOI: 10.17632/x7sg4kgv8s.1.

Conflict of Interest

All authors declare that they have no conflict of interest.

References

[1] J. Burisch, J. Claytor, I. Hernandez, et al., The Cost of Inflammatory Bowel Disease Care - How to Make it Sustainable, Clin Gastroenterol Hepatol. (2024) https://doi.org/10.1016/j.cgh.2024.06.049.

[2] B. Wu, S. Su, Y. Li, et al., Dysregulated programmed cell death of intestinal epithelial cells in ulcerative colitis: Molecular mechanisms and novel therapeutic interventions (Review), Int J Mol Med. 56 (2025) https://doi.org/10.3892/ijmm.2025.5671.

[3] J.C. Pérez, The interplay between gut bacteria and the yeast Candida albicans, Gut Microbes. 13 (2021) 1979877. https://doi.org/10.1080/19490976.2021.1979877.

[4] M. Fassarella, E.E. Blaak, J. Penders, et al., Gut microbiome stability and resilience: elucidating the response to perturbations in order to modulate gut health, Gut. 70 (2021) 595-605. https://doi.org/10.1136/gutjnl-2020-321747.

[5] C.L. Hsu, B. Schnabl, The gut-liver axis and gut microbiota in health and liver disease, Nat Rev Microbiol. 21 (2023) 719-733. https://doi.org/10.1038/s41579-023-00904-3.

[6] E.A. Franzosa, A. Sirota-Madi, J. Avila-Pacheco, et al., Gut microbiome structure and metabolic activity in inflammatory bowel disease, Nat Microbiol. 4 (2019) 293-305. https://doi.org/10.1038/s41564-018-0306-4.

[7] C. Foppa, T. Rizkala, A. Repici, et al., Microbiota and IBD: Current knowledge and future perspectives, Dig Liver Dis. 56 (2024) 911-922. https://doi.org/10.1016/j.dld.2023.11.015.

[8] M.-X. Li, M.-Y. Li, J.-X. Lei, et al., Huangqin decoction ameliorates DSS-induced ulcerative colitis: Role of gut microbiota and amino acid metabolism, mTOR pathway and intestinal epithelial barrier, Phytomedicine. 100 (2022) 154052. https://doi.org/10.1016/j.phymed.2022.154052.

[9] Y. Dong, H. Fan, Z. Zhang, et al., Berberine ameliorates DSS-induced intestinal mucosal barrier dysfunction through microbiota-dependence and Wnt/β-catenin pathway, Int J Biol Sci. 18 (2022) 1381-1397. https://doi.org/10.7150/ijbs.65476.

[10] N. Díaz-Garrido, J. Badia, L. Baldomà, Microbiota-derived extracellular vesicles in interkingdom communication in the gut, J Extracell Vesicles. 10 (2021) e12161. https://doi.org/10.1002/jev2.12161.

[11] K.C.P. Cheung, M. Jiao, C. Xingxuan, et al., Extracellular vesicles derived from host and gut microbiota as promising nanocarriers for targeted therapy in osteoporosis and osteoarthritis, Front Pharmacol. 13 (2022) 1051134. https://doi.org/10.3389/fphar.2022.1051134.

[12] J. Huang, X. Wang, Z. Wang, et al., Extracellular vesicles as a novel mediator of interkingdom communication, Cytokine Growth Factor Rev. 73 (2023) 173-184. https://doi.org/10.1016/j.cytogfr.2023.08.005.

[13] L. Fizanne, A. Villard, N. Benabbou, et al., Faeces-derived extracellular vesicles participate in the onset of barrier dysfunction leading to liver diseases, J Extracell Vesicles. 12 (2023) e12303. https://doi.org/10.1002/jev2.12303.

[14] K.-S. Park, J. Lee, C. Lee, et al., Sepsis-Like Systemic Inflammation Induced by Nano-Sized Extracellular Vesicles From Feces, Front Microbiol. 9 (2018) 1735. https://doi.org/10.3389/fmicb.2018.01735.

[15] A. Kumar, K. Sundaram, J. Mu, et al., High-fat diet-induced upregulation of exosomal phosphatidylcholine contributes to insulin resistance, Nat Commun. 12 (2021) 213. https://doi.org/10.1038/s41467-020-20500-w.

[16] E.Y. Chen, S. Mahurkar-Joshi, C. Liu, et al., The Association Between a Mediterranean Diet and Symptoms of Irritable Bowel Syndrome, Clin Gastroenterol Hepatol. 22 (2024) https://doi.org/10.1016/j.cgh.2023.07.012.

[17] M. Zu, G. Liu, H. Xu, et al., Extracellular Vesicles from Nanomedicine-Trained Intestinal Microbiota Substitute for Fecal Microbiota Transplant in Treating Ulcerative Colitis, Adv Mater. 36 (2024) e2409138. https://doi.org/10.1002/adma.202409138.

[18] J.P. Baixinho, J.D. Anastácio, V. Ivasiv, et al., Supercritical CO2 Extraction as a Tool to Isolate Anti-Inflammatory Sesquiterpene Lactones from Cichorium intybus L. Roots, Molecules. 26 (2021) https://doi.org/10.3390/molecules26092583.

[19] X.-H. Meng, Y.-A. Pan, H. Lv, et al., One new 12, 8-guaianolide sesquiterpene lactone with antihyperglycemic activity from the roots of Cichorium intybus, Nat Prod Res. 38 (2023) 3244-3252. https://doi.org/10.1080/14786419.2023.2230606.

[20] J. Perović, V. Tumbas Šaponjac, J. Kojić, et al., Chicory (Cichorium intybus L.) as a food ingredient - Nutritional composition, bioactivity, safety, and health claims: A review, Food Chem. 336 (2020) 127676. https://doi.org/10.1016/j.foodchem.2020.127676.

[21] Y. Tian, T. Jian, J. Li, et al., Phenolic acids from Chicory roots ameliorate dextran sulfate sodium-induced colitis in mice by targeting TRP signaling pathways and the gut microbiota, Phytomedicine. 128 (2024) 155378. https://doi.org/10.1016/j.phymed.2024.155378.

[22] Y. Zhou, T. Wen, S. Yang, et al., Sesquiterpene lactones from Cichorium intybus exhibit potent anti-inflammatory and hepatoprotective effects by repression of NF-κB and enhancement of NRF2, J Ethnopharmacol. 343 (2025) 119439. https://doi.org/10.1016/j.jep.2025.119439.

[23] L. Huang, Z. Zhang, F. Zhang, et al., Amelioration of metabolic syndrome in high-fat diet-fed mice by total sesquiterpene lactones of chicory via modulation of intestinal flora and bile acid excretion, Food Funct. 16 (2025) 1830-1846. https://doi.org/10.1039/d4fo05633g.

[24] Y. Pan, H. Zhang, M. Li, et al., Novel approaches in IBD therapy: targeting the gut microbiota-bile acid axis, Gut Microbes. 16 (2024) 2356284. https://doi.org/10.1080/19490976.2024.2356284.

[25] Y. Zhong, H. Emam, W. Hou, et al., Cichorium glandulosum Ameliorates HFD-Induced Obesity in Mice by Modulating Gut Microbiota and Bile Acids, J Med Food. 27 (2024) 601-614. https://doi.org/10.1089/jmf.2024.k.0030.

[26] B.E. Kase, A.D. Liese, J. Zhang, et al., The Development and Evaluation of a Literature-Based Dietary Index for Gut Microbiota, Nutrients. 16 (2024) https://doi.org/10.3390/nu16071045.

[27] J. Peng, H. Li, O.A. Olaolu, et al., Natural Products: A Dependable Source of Therapeutic Alternatives for Inflammatory Bowel Disease through Regulation of Tight Junctions, Molecules. 28 (2023) https://doi.org/10.3390/molecules28176293.

[28] C. Christensen, A. Knudsen, E.K. Arnesen, et al., Diet, Food, and Nutritional Exposures and Inflammatory Bowel Disease or Progression of Disease: an Umbrella Review, Adv Nutr. 15 (2024) 100219. https://doi.org/10.1016/j.advnut.2024.100219.

[29] R. Rivera Rodríguez, J.J. Johnson, Terpenes: Modulating anti-inflammatory signaling in inflammatory bowel disease, Pharmacol Ther. 248 (2023) 108456. https://doi.org/10.1016/j.pharmthera.2023.108456.

[30] J. Perović, V. Tumbas Šaponjac, J. Kojić, et al., Chicory (Cichorium intybus L.) as a food ingredient - Nutritional composition, bioactivity, safety, and health claims: A review, Food Chem. 336 (2021) 127676. https://doi.org/10.1016/j.foodchem.2020.127676.

[31] X.-H. Meng, H. Lv, X.-Q. Ding, et al., Sesquiterpene lactones with anti-inflammatory and cytotoxic activities from the roots of Cichorium intybus, Phytochemistry. 203 (2022) 113377. https://doi.org/10.1016/j.phytochem.2022.113377.

[32] X.-H. Meng, Y.-A. Pan, H. Lv, et al., One new 12, 8-guaianolide sesquiterpene lactone with antihyperglycemic activity from the roots of Cichorium intybus, Nat Prod Res. 38 (2024) 3244-3252. https://doi.org/10.1080/14786419.2023.2230606.

[33] S.-M. Pan, C.-L. Wang, Z.-F. Hu, et al., Baitouweng decoction repairs the intestinal barrier in DSS-induced colitis mice via regulation of AMPK/mTOR-mediated autophagy, J Ethnopharmacol. 318 (2024) 116888. https://doi.org/10.1016/j.jep.2023.116888.

[34] K. Liu, Y. Yin, C. Shi, et al., Asiaticoside ameliorates DSS-induced colitis in mice by inhibiting inflammatory response, protecting intestinal barrier and regulating intestinal microecology, Phytother Res. 38 (2024) 2023-2040. https://doi.org/10.1002/ptr.8129.

[35] M.V. Bénard, M.C. de Goffau, J. Blonk, et al., Fecal Microbiota Transplantation Outcome and Gut Microbiota Composition in Ulcerative Colitis: A Systematic Review and Meta-Analysis, Clin Gastroenterol Hepatol. (2024) https://doi.org/10.1016/j.cgh.2024.10.001.

[36] Q. Hu, Z. Hu, X. Yan, et al., Extracellular vesicles involved in growth regulation and metabolic modulation in Haematococcus pluvialis, Biotechnol Biofuels Bioprod. 17 (2024) 15. https://doi.org/10.1186/s13068-024-02462-z.

[37] T. Chen, B. Zhang, G. He, et al., Gut-Derived Exosomes Mediate the Microbiota Dysbiosis-Induced Spermatogenesis Impairment by Targeting Meioc in Mice, Adv Sci (Weinh). 11 (2024) e2310110. https://doi.org/10.1002/advs.202310110.

[38] J. Verbunt, J. Jocken, E. Blaak, et al., Gut-bacteria derived membrane vesicles and host metabolic health: a narrative review, Gut Microbes. 16 (2024) 2359515. https://doi.org/10.1080/19490976.2024.2359515.

[39] C. Zheng, Y. Zhong, W. Zhang, et al., Chlorogenic Acid Ameliorates Post-Infectious Irritable Bowel Syndrome by Regulating Extracellular Vesicles of Gut Microbes, Adv Sci (Weinh). 10 (2023) e2302798. https://doi.org/10.1002/advs.202302798.

[40] Q. Shen, Z. Huang, J. Yao, et al., Extracellular vesicles-mediated interaction within intestinal microenvironment in inflammatory bowel disease, J Adv Res. 37 (2022) 221-233. https://doi.org/10.1016/j.jare.2021.07.002.

[41] X. Qin, Z. Liu, K. Nong, et al., Porcine-derived antimicrobial peptide PR39 alleviates DSS-induced colitis via the NF-κB/MAPK pathway, Int Immunopharmacol. 127 (2024) 111385. https://doi.org/10.1016/j.intimp.2023.111385.

[42] Y. Yan, Y. Lei, Y. Qu, et al., Bacteroides uniformis-induced perturbations in colonic microbiota and bile acid levels inhibit TH17 differentiation and ameliorate colitis developments, NPJ Biofilms Microbiomes. 9 (2023) 56. https://doi.org/10.1038/s41522-023-00420-5.

[43] Y. Wu, L. Ran, Y. Yang, et al., Deferasirox alleviates DSS-induced ulcerative colitis in mice by inhibiting ferroptosis and improving intestinal microbiota, Life Sci. 314 (2023) 121312. https://doi.org/10.1016/j.lfs.2022.121312.

[44] Z.-Y. Chang, H.-M. Liu, Y.-L. Leu, et al., Modulation of Gut Microbiota Combined with Upregulation of Intestinal Tight Junction Explains Anti-Inflammatory Effect of Corylin on Colitis-Associated Cancer in Mice, Int J Mol Sci. 23 (2022) https://doi.org/10.3390/ijms23052667.

[45] W.-W. Zhang, K. Thakur, J.-G. Zhang, et al., Riboflavin ameliorates intestinal inflammation via immune modulation and alterations of gut microbiota homeostasis in DSS-colitis C57BL/6 mice, Food Funct. 15 (2024) 4109-4121. https://doi.org/10.1039/d4fo00835a.

[46] W. Niu, Y. Chen, L. Wang, et al., The combination of sodium alginate and chlorogenic acid enhances the therapeutic effect on ulcerative colitis by the regulation of inflammation and the intestinal flora, Food Funct. 13 (2022) 10710-10723. https://doi.org/10.1039/d2fo01619b.

[47] Y. Luo, S. Fu, Y. Liu, et al., Banxia Xiexin decoction modulates gut microbiota and gut microbiota metabolism to alleviate DSS-induced ulcerative colitis, J Ethnopharmacol. 326 (2024) 117990. https://doi.org/10.1016/j.jep.2024.117990.

[48] H. Gu, Y. Tian, J. Xia, et al., Li-Hong Tang alleviates dextran sodium sulfate-induced colitis by regulating NRF2/HO-1 signaling pathway and gut microbiota, Front Pharmacol. 15 (2024) 1413666. https://doi.org/10.3389/fphar.2024.1413666.

[49] S. Rome, S. Tacconi, High-fat diets: You are what you eat….your extracellular vesicles too!, J Extracell Vesicles. 13 (2024) e12382. https://doi.org/10.1002/jev2.12382.

[50] J. Wang, L. Li, Z. Zhang, et al., Extracellular vesicles mediate the communication of adipose tissue with brain and promote cognitive impairment associated with insulin resistance, Cell Metab. 34 (2022) https://doi.org/10.1016/j.cmet.2022.08.004.

[51] P. Margutti, A. D'Ambrosio, S. Zamboni, Microbiota-Derived Extracellular Vesicle as Emerging Actors in Host Interactions, Int J Mol Sci. 25 (2024) https://doi.org/10.3390/ijms25168722.

[52] S. Zhang, Q. Wang, D.E.L. Tan, et al., Gut-liver axis: Potential mechanisms of action of food-derived extracellular vesicles, J Extracell Vesicles. 13 (2024) e12466. https://doi.org/10.1002/jev2.12466.

[53] M. Jiang, Y. Jike, K. Liu, et al., Exosome-mediated miR-144-3p promotes ferroptosis to inhibit osteosarcoma proliferation, migration, and invasion through regulating ZEB1, Mol Cancer. 22 (2023) 113. https://doi.org/10.1186/s12943-023-01804-z.

[54] M.-J. Kim, S.-G. Lim, D.-H. Cho, et al., Regulation of inflammatory response by LINC00346 via miR-25-3p-mediated modulation of the PTEN/PI3K/AKT/NF-κB pathway, Biochem Biophys Res Commun. 709 (2024) 149828. https://doi.org/10.1016/j.bbrc.2024.149828.

[55] X.-Y. Luo, J.-H. Ying, Q.-S. Wang, miR-25-3p ameliorates SAE by targeting the TLR4/NLRP3 axis, Metab Brain Dis. 37 (2022) 1803-1813. https://doi.org/10.1007/s11011-022-01017-1.

[56] Q. Shen, Z. Huang, L. Ma, et al., Extracellular vesicle miRNAs promote the intestinal microenvironment by interacting with microbes in colitis, Gut Microbes. 14 (2022) 2128604. https://doi.org/10.1080/19490976.2022.2128604.

[57] S. Min, W. Tao, Y. Miao, et al., Dual Delivery of Tetramethylpyrazine and miR-194-5p Using Soft Mesoporous Organosilica Nanoparticles for Acute Lung Injury Therapy, Int J Nanomedicine. 18 (2023) 6469-6486. https://doi.org/10.2147/IJN.S420802.

[58] R. Wang, Q.-Y. Wang, Y. Bai, et al., Research progress of diabetic retinopathy and gut microecology, Front Microbiol. 14 (2023) 1256878. https://doi.org/10.3389/fmicb.2023.1256878.

[59] J. Zhao, G. Song, F. Weng, et al., The choleretic role of tauroursodeoxycholic acid exacerbates alpha-naphthylisothiocyanate induced cholestatic liver injury through the FXR/BSEP pathway, J Appl Toxicol. 43 (2023) 1095-1103. https://doi.org/10.1002/jat.4446.

[60] A. Weiss, K. Alack, S. Klatt, et al., Sustained Endurance Training Leads to Metabolomic Adaptation, Metabolites. 12 (2022) https://doi.org/10.3390/metabo12070658.

[61] L. Bao, D. Hao, X. Wang, et al., Transcriptome investigation of anti-inflammation and immuno-regulation mechanism of taurochenodeoxycholic acid, BMC Pharmacol Toxicol. 22 (2021) 23. https://doi.org/10.1186/s40360-021-00491-0.

[62] J. Cai, L. Sun, F.J. Gonzalez, Gut microbiota-derived bile acids in intestinal immunity, inflammation, and tumorigenesis, Cell Host Microbe. 30 (2022) 289-300. https://doi.org/10.1016/j.chom.2022.02.004.

[63] S.R. Sinha, Y. Haileselassie, L.P. Nguyen, et al., Dysbiosis-Induced Secondary Bile Acid Deficiency Promotes Intestinal Inflammation, Cell Host Microbe. 27 (2020) https://doi.org/10.1016/j.chom.2020.01.021.

[64] L. Ma, Q. Shen, W. Lyu, et al., Clostridium butyricum and Its Derived Extracellular Vesicles Modulate Gut Homeostasis and Ameliorate Acute Experimental Colitis, Microbiol Spectr. 10 (2022) e0136822. https://doi.org/10.1128/spectrum.01368-22.

[65] L. Ma, W. Lyu, Y. Song, et al., Anti-Inflammatory Effect of Clostridium butyricum-Derived Extracellular Vesicles in Ulcerative Colitis: Impact on Host microRNAs Expressions and Gut Microbiome Profiles, Mol Nutr Food Res. 67 (2023) e2200884. https://doi.org/10.1002/mnfr.202200884.

[66] J. Park, N.-E. Kim, H. Yoon, et al., Fecal Microbiota and Gut Microbe-Derived Extracellular Vesicles in Colorectal Cancer, Front Oncol. 11 (2021) 650026. https://doi.org/10.3389/fonc.2021.650026.

[67] R. Wang, Y. Yang, J. Liang, et al., Tetrahedral Framework Nucleic Acid-Based Delivery of miR-34a Inhibitor for the Treatment of Metabolic Dysfunction-Associated Steatohepatitis, ACS Appl Mater Interfaces. (2025) https://doi.org/10.1021/acsami.5c18832.

[68] G. Jia, J. Li, M. Jiang, et al., Unraveling the miR-144-3p/PUMA pathway: a novel regulator of FDX1-mediated cuproptosis in colorectal cancer, Cell Oncol (Dordr). (2025) https://doi.org/10.1007/s13402-025-01093-2.